

IGF-1: AN IN VITRO SKELETAL MUSCLE CELL MODE OF EXERCISE MIMETICS TO INVESTIGATE THE ROLE OF EXOSOMAL TRAFFICKING IN REGULATING METABOLIC RESPONSES TO EXERCISE

WRITTEN BY MARINA FORTE

SUPERVISOR: PROF PHILIP ATHERTON
CO- SUPERVISOR: PROF KENNETH SMITH
CO- SUPERVISOR: DR DANIEL WILKINSON

THIS THESIS IS SUBMITTED TO THE UNIVERSITY OF NOTTINGHAM FOR THE DEGREE OF MRES

MAY 2019

Table of contents

TABLE OF CONTENTS **2**

INDEX OF FIGURES **3**

INDEX OF TABLES **3**

ABSTRACT **4**

ACKNOWLEDGEMENTS **5**

INTRODUCTION **6**

Skeletal muscle structure and function 6

Basic structure of a muscle *6*

The endoplasmic reticulum and Golgi complex crosstalk 7

Exercise 7

Benefits of regular exercise go beyond the sole muscles involved *7*

Emulating exercise *8*

The C2C12 muscle cell line 11

Insulin-like Growth Factor 1 11

Exo1 13

Aims 13

MATERIALS AND METHODS **14**

Cell culture 14

Experimental design *14*

IGF-1 treatment *14*

Harvesting *15*

Analysis tools 16

Western blotting *16*

Protein/DNA ratio *19*

Myotube diameter measurement *20*

Picture taking method 20

Digital measurement method 20

Statistical analysis 22

RESULTS **23**

Myotube width is increased at 24h in both treated groups and is decreased at 48h by Exo1 addition. 25

Exo1 increases pMAPK-Erk1/2 (Thr202/Tyr204 and Thr185/Tyr187) phosphorylation at 24h but decreases it at 48h. 25

Akt phosphorylation at Ser473 is increased by IGF-1 and boosted by Exo1. 25

PmTOR (Ser4228) is upregulated by IGF-1 at 48h and downregulated by Exo1. 25

Exo1 affects 4EBP1 phosphorylation at Thr37/46 at 24h, while IGF-1 only affects it at 48h. 25

Exo1 increases phosphorylation of eEF2 (Thr56) at 24h 25

IGF-1 treatment increases ASP per DNA unit at 48h. Exo1 addition increases dsDNA at 24h and boosts protein synthesis per DNA unit at 48h 26

DISCUSSION **27**

IGF-1 treatment enhances hypertrophy at the earlier 24h time point through activation of mTORC2 and follows up with mTORC1 at 48h. 27

ER stress induced by IGF-1+Exo1 elicits hypertrophy at 24h, but the effect is blunted after 48h. 30

CONCLUSION **32**

REFERENCES **33**

APPENDICES **39**

Appendix 1: preparation of reagents 39

PBS *39*

Exo1 ..... *39*
IGF-1 ..... *39*
Homogenisation buffer *39*
Laemmli SDS sample buffer *40*
Transfer buffer *40*
TBST *40*
Coomassie stain *40*
APPENDIX 2: PROTEIN/DNA ANALYSIS 41
Total protein 41
Total dsDNA 41
protein/DNA 41
APPENDIX 3: ESTIMATED MARGINAL MEANS OF WESTERN BLOTTING AND MYOTUBE WIDTH RESULTS 42

Index of figures

FIGURE 2 PROPOSED MECHANISM OF ACTION OF RESVERATROL AND EFFECTS OBSERVED 10
FIGURE 1 PICTURE TAKING METHOD. EACH BLUE RECTANGLE REPRESENTS THE AREA IN WHICH A PICTURE WAS TAKEN. 20
FIGURE 2 DIGITAL MEASUREMENT METHOD FOR EVERY MYOTUBE. 21
FIGURE 3. DIGITAL ANALYSIS OF THE MYOTUBE WIDTH FOLLOWING IGF-1±EXO1 TREATMENT [A]. WESTERN BLOTTING, EXPRESSION OF PMAPK_P44/ERK1 [B_1] AND PMAPK_P42/ERK2 [B_2], AKT PHOSPHORYLATION AT SER473 [C], MTOR PHOSPHORYLATION AT SER4228 [D], EXPRESSION OF P4EBP1-15KDA [E_1] AND P4EBP1-20KDA [E_2] EXPRESSION OF PEEF2 (THR56) [F]. 24
FIGURE 4 TOTAL PROTEIN, TOTAL DNA AND PROTEIN/DNA RATIO ANALYSIS FOLLOWING IGF-1±EXO1 TREATMENT. [A]TOTAL PROTEIN EXPRESSION (MG). [B] ESTIMATED MARGINAL MEANS FOR TOTAL PROTEIN EXPRESSION (MG). [C] TOTAL DOUBLE STRANDED DNA EXPRESSION (µG). [D] ESTIMATED MARGINAL MEANS FOR TOTAL DSDNA EXPRESSION (µG). [E] PROTEIN/DNA RATIO (µG/µG). [F] ESTIMATED MARGINAL MEANS FOR PROTEIN/DNA RATIO (µG/µG). 41
FIGURE 5 ESTIMATED MARGINAL MEANS OF PMAPK_P4 [A_1] PMAPK_P42 [A_2] PAKT [B] PMTOR [C] P4EBP1-20KDA[D_1] P4EBP1-15KDA[D_2] PEEF2[E]. 42
FIGURE 6 ESTIMATED MARGINAL MEANS OF MYOTUBE WIDTH FOLLOWING IGF-1±EXO1 TREATMENT. 43

Index of tables

TABLE 1TOTAL PROTEIN, TOTAL DNA AND PROTEIN/DNA RATIO ANALYSIS. RESULTS ARE EXPRESSED AS MEAN ± SD. ASTERISKS INDICATE A SIGNIFICANT DIFFERENCE ($P<0.05$) 26
TABLE 2MAIN FINDINGS FROM IGF-1 AND IGF-1+EXO1 TREATMENT OF C2C12 CELLS FOR 24 AND 48H. 27

Abstract

Exercise mimetics are pharmacological compounds that trigger pathways similar to those activated as a consequence of exercise training. They are therefore useful in pathological conditions where physical activity is beneficial but unfeasible. Models of exercise mimetics can also be used to study the targets implicated in training or conversely, inactivity. In the study presented insulin-like growth factor-1 (IGF-1) is investigated as an in vitro model of exercise mimetics, plus or minus the addition of Exo1 drug, that should impair the crosstalk between endoplasmic reticulum and the Golgi apparatus to inquire in its role in exercise metabolism

In this study, cultures from the murine musculoskeletal cell line C2C12 are divided into three experimental groups for each exercise mimetics: a control group, a treated group and a treated group plus Exo1. Cells are treated for 24h and 48h.

IGF-1 increased myotube width at 24h by eliciting mTORC2, followed by mTORC1 at 48h. Hypertrophy was achieved independently of pMAPK.

IGF-1 overcompensated for Exo1-caused ER stress by inducing hypertrophy at 24h, but the effect was impaired after 48h. Hypertrophy at 24h was achieved through phosphorylation of ERK1/2 and pAkt.

Acknowledgements

To my supervisors for their experience and guidance.

To my colleagues and fellow students for their patience and support.

To my family, near or far, for every day of my life.

Introduction

Skeletal muscle structure and function

Basic structure of a muscle

The basic structural unit of the skeletal muscle is called a muscle fibre. This is the result of the fusion of many undifferentiated, mononucleated cells, known as myoblasts, forming a cylindrical multi-nucleated cell. Such process is called differentiation, and it is completed by the time of birth (Vander, Sherman and Luciano, 2001).

Fibres keep augmenting in size until adulthood, but do not increase their number. However, undifferentiated satellite cells, located adjacently to the existing fibres can undergo differentiation and form new fibres to replace those damaged as a result of injury (Vander, Sherman and Luciano, 2001).

A muscle is formed by a multitude of fibres bound together in fascicles by connective tissue. Various bundles, interspersed with blood vessels, are then clustered together by further layers of connective tissue. The muscle is, in turn, linked to bones by tendons, which are bundles of collagen fibre (Vander, Sherman and Luciano, 2001).

Typical of this voluntary muscle, as well as of cardiac muscle, is its striated appearance. This is due to the arrangement of actin and myosin filaments into a repeated pattern along cylindrical bundles, called myofibrils. Each repeated pattern is connected to the other by a network of proteins known as the Z line, which is directly anchored to actin. Overlapping to actin instead, are the thicker myosin filaments. These latter are, in turn, linked together by proteins, in an area known as the M line. Connecting the M to the Z line are filaments of titin protein (Cooper, 2000). The whole structure is therefore thoroughly connected and no element of it is free-floating (Vander, Sherman and Luciano, 2001).

Small projections arise from myosin filaments in the area where these overlap with actin. The projections have the shape of two globular heads, attached to the heavy chains of each myosin molecule, and are orientated towards actin (Squire, 2016).

A unit of this repeated pattern, delimited by two Z lines, is called a sarcomere.

To better explain the terminology of the muscle, a summary of the structural terms follows:

- A band: a region, central to the sarcomere, of dark appearance, composed of myosin filaments
- I bands: areas flanking the A band at each side, and contrasting with it for their lighter appearance, composed of those portions of actin that do not overlap with myosin
- H zone: area comprised within the A band where the myosin filaments are not overlapped by actin
- Z lines: regions bisecting each I band and composed of a network of proteins that bind actin
- M line: narrow, dark band of proteins that link together the central portion of myosin filaments, at the centre of the H zone (Vander, Sherman and Luciano, 2001)
- Titin: protein filaments extending from the M to the Z line (Cooper, 2000)
- Sarcomere: area comprised within two Z lines and basic contractile unit of the muscle.

The endoplasmic reticulum of muscles is specifically called sarcoplasmic reticulum, and it forms segments of sleeve-like structures surrounding each myofibril: one segment surrounds the A band, another segment the I band, and are connected by smaller tubular structures called transversal (T) tubes (Vander, Sherman and Luciano, 2001).

The function of the endoplasmic (or sarcoplasmic) reticulum will be discussed in further detail in the relevant section below.

The endoplasmic reticulum and Golgi complex crosstalk

The endoplasmic reticulum (ER) is the organelle in which lipids and proteins are synthesised. It can be divided into two types, both present in the cell in different proportions: the granular endoplasmic reticulum, carrying the protein producing ribosomes on its surface and standing at the interface between the nuclear membrane and the Golgi apparatus, and the agranular endoplasmic reticulum, a branched tubular network of membranes in which lipid molecules are synthesized and calcium ions (Ca^{2+}) are stored for release and regulation of various cell functions (Vander, Sherman and Luciano, 2001; English and Voeltz, 2013).

The proteins produced bud out of the endoplasmic reticulum, packaged in secretory vesicles that are then transferred to the Golgi apparatus (or Golgi complex GC). Most of the post-translational modifications occur in this other membranous system which then sorts the synthesised components into new secretory vesicles to be transported into the cytoplasm to their target organelles or to the plasma membrane and into the extracellular environment in a process known as exocytosis (Vander, Sherman and Luciano, 2001; Barone *et al.*, 2015)

The ER and GC undergo a profound reorganisation during skeletal muscle cell differentiation, thus also remodelling their secretory pathways. The ER junctional regions specialise into calcium release during contraction, while longitudinal regions perform calcium uptake (Barone *et al.*, 2015). The GC, instead undergoes fragmentation and organises in a fibre type-dependent fashion. In slow twitch fibres 75% of the GC elements gather around the nucleus, whereas in type IIB fast twitch fibres most of the GC fragments are in the fibre core while nuclei only have some elements placed at their poles (Ralston, Lu and Ploug, 1999).

Exercise

Benefits of regular exercise go beyond the sole muscles involved

Exercise relies on many signalling pathways that overall promote and maintain metabolic health (Safdar, Saleem and Tarnopolsky, 2016). One of its major effect is the attenuation of myostatin, a protein involved in the modulation of adipose tissue mass and function, as shown in both human and rodent models (Pedersen and Febbraio, 2012).

Over time, skeletal muscle regularly undergoing training presents mechanisms of adaptation that are able to condition the substrate used to produce energy, becoming less reliant on glucose and sensitising adipose tissue to lipolysis and fatty acid oxidation (Pedersen and Febbraio, 2012).

Research in the past two decades has established muscle as an endocrine organ (Pedersen and Febbraio, 2012), capable of secreting factors during its activity that trigger many plastic changes within and beyond the skeletal muscle itself (Handschin, 2016). The same team produced a review suggesting that, for this reason, cytokines and other peptides produced by muscle fibres and exerting either autocrine, paracrine or endocrine effects should be specifically classed as myokines (Pedersen *et al.*, 2003).

Most factors secreted by adipocytes are pro-inflammatory, correlating well with development of obesity induced metabolic and cardiovascular disorders (Pedersen and Febbraio, 2012). Recent research has been focused on finding protective factors against these harmful effects and myokines are a strong candidate to provide a counterbalance to adipokines (Pedersen and Febbraio, 2012). Lambernd *et al.* (2012) even established how contractile activity not only counterbalances, but directly inhibits pro-inflammatory signalling pathways.

Physical activity, in fact, holds a strong correlation with increased healthspan and life expectancy in humans (Handschin, 2016). By contrast, muscle inactivity leads to a loss in insulin sensitivity (Lambernd *et al.*, 2012) and antioxidative capacity and consequent accumulation of reactive oxygen species (ROS) (Chen, Barberio and Hubal, 2016). Oxidative stress is correlated with the onset of sarcopenia, dysregulation of vessel role (Dillon, 2016)muscle loss (Barreiro and Gea, 2016) and diabetes (Evers-van Gogh *et al.*, 2015).

Given the insulin-independent nature of muscle glucose uptake during exercise, any insulin signalling deficiencies that are known to cause chronic conditions are circumvented (Lambernd *et al.*, 2012).

Particularly, in ageing individuals, training lessens oxidative stress and damage in adipose tissue, kidney, brain and liver, which further highlights the correlation between exercise and overall health (Safdar, Saleem and Tarnopolsky, 2016).

The study by Kanzleiter *et al.* (2014) establishes decorin, a proteoglycan whose function has been better investigated in tendons than in skeletal muscle, as an exercise-regulated myokine, secreted during muscle contraction and involved in hypertrophy and muscle reconstruction. Coupled with its expression, myostatin and the catabolic pathways associated with it appear to be suppressed (Kishioka *et al.*, 2008).

Meta-analysis studies by Nocon *et al.(*2008) and Wolin *et al.* (2009) show, respectively, a decrease in the risk of cardiovascular disease and all-cause mortality between 33% and 35% and a decrease by 24% of the risk of colon cancer in active individuals, as opposed to inactive population subgroups.

Physical activity has also been shown to regulate bone maintenance through accumulation of mineral and consequent increase of bone mineral density (BMD). The coupling of increased bone density and muscle strength and improvement of balance altogether reduces the risk of osteoporosis and fractures (Borer, 2005).

Regular physical activity therefore has health promoting effects that span from the prevention of chronic metabolic diseases —type two diabetes, obesity, cardiovascular disease, to cite some — to mental health conditions such as depression and dementia (Lambernd *et al.*, 2012; Safdar, Saleem and Tarnopolsky, 2016). In fact, it has been shown to promote hippocampal neurogenesis and neuronal plasticity, and to counter age-related cognitive decline as well as neurodegenerative diseases (Guerrieri, Moon and van Praag, 2017).

Emulating exercise

Other than preventing chronic disease, physical activity has also been shown to increase survival and improve the quality of life of cancer patients (Montazeri, 2008). It is not, however, always possible to prescribe exercise to patients with such severe pathological conditions. Exercise mimetics are pharmacological compounds developed as a means to triggering cell signalling pathways analogous to those verified during and after exercise

(Pigna *et al.*, 2016). These drugs can therefore be used as a complement to training: the so-called exercise pill, a concept first defined this way by (Goodyear, 2008).

At a level of basic research, models of exercise mimetics could also be exploited for the identification of pharmacological targets implicated in metabolic processes related to either physical activity or absence of the same (Lambernd *et al.*, 2012). The study and development of in vitro models may help overcome the practical and ethical issues of in vivo investigations (Booth and Laye, 2009), in addition to being key steps prior to administration to patients.

However, it has to be remembered that the array of beneficial effects of physical activity is vast and complex, and therefore cannot be achieved by means of a single pill, nor can a pill be effective as the sole treatment of complex diseases. Exercise mimetics is not a substitute for an active lifestyle. Moreover, many of the compounds such as the ones widely used to enhance athletic performances can produce life-threatening effects (Handschin, 2016), hence the need to identify other targets and pharmacological interventions.

The activation of signalling pathways relevant to energy metabolism, like the AMPK-SIRT1-PGC-1α pathway, is one of the main targets of research into exercise mimetics (Guerrieri, Moon and van Praag, 2017). Sirtuin (SIRT1) is sensitive to the changes in NAD^+ verified during muscle contraction and, in response, it is capable of regulating a large number of downstream targets including AMPK and PGC-1α, the main regulators, in turn, of muscle energy metabolism and mitochondrial biogenesis (Barbieri *et al.*, 2011; Das *et al.*, 2012; Guerrieri, Moon and van Praag, 2017).

5-aminoimidazole-4-carboxyamide ribonucleoside (AICAR) is one important and widely studied exercise mimetics. AICAR is a potent stimulator of AMPK, a kinase involved in the negative regulation of muscle mass (Egawa *et al.*, 2014).

The study by Egawa and colleagues shows that AMPK inhibits hypertrophy through downregulation of Heat shock proteins (HSP), thus favouring protein degradative pathways (Egawa *et al.*, 2014). HSP are stress-induced molecules that play a role in maintaining correct protein folding and transport in a cytoprotective fashion and are involved in muscle adaptation to exercise (Welc *et al.*, 2012; Egawa *et al.*, 2014).

AMPK activation during exercise is also associated with an activation of eEF2K and 4EBP1, which actively inhibit protein translation, together with changes in the mTORC1 complex assembly, that again hinder protein synthesis (Rose *et al.*, 2009).

AMPK also plays an important role in insulin sensitivity as a consequence of exercise and, although the mechanisms have to be clarified, it appears to act through reduction of ER stress (Boulinguiez *et al.*, 2017).

A concept that runs in parallel with exercise mimetics is that of "caloric restriction mimetics", which comprises yet other drugs (Richter, Kiens and Wojtaszewski, 2008; Handschin, 2016).

Resveratrol, for instance, is a natural occurring compound widely found in human diet. Its highly lipophilic composition means it is able to cross the cell membrane and interact with its receptors (Guerrieri, Moon and van Praag, 2017).

Resveratrol has pleiotropic effects on both skeletal muscle and brain. In skeletal muscle, it upregulates pathways involved in endurance, fatty acid oxidation of white adipose tissue, insulin sensitivity and mitochondrial biogenesis by means of AMPK activation (Handschin,

2016; Fan and Evans, 2017; Guerrieri, Moon and van Praag, 2017). AMPK raises the level of NAD+, that acts as a substrate for SIRT1, which in turn activates PGC1α and ultimately PPARδ (Fan and Evans, 2017). summarises the process.

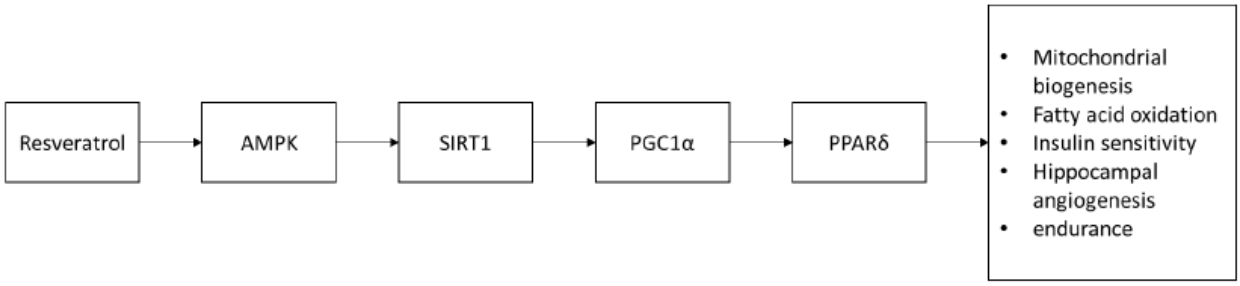


Figure 1 Proposed mechanism of action of Resveratrol and effects observed

In the brain, resveratrol affects vasodilation and angiogenesis in the hippocampus (Guerrieri, Moon and van Praag, 2017). During cell respiration, it acts as a modulator of complex I of the respiratory chain (Handschin, 2016).

As a dietary supplement to exercise trained rodents, this compound was observed to alleviate exercise-induced oxidative stress damage (Guerrieri, Moon and van Praag, 2017). Evidence seems to point resveratrol as a performance enhancer in the presence of exercise in mice model, but, surprisingly, it has been shown to blunt training adaptation effects in humans (Handschin, 2016; Guerrieri, Moon and van Praag, 2017). What's more, there is contradictory documentation concerning its efficacy alone, not in presence of exercise (Guerrieri, Moon and van Praag, 2017). Because its mechanisms of action remain elusive, more research is required to establish suitable intake dosages.

The C2C12 muscle cell line

Yaffe and Saxel (1977) first established the C2 cell line from healthy mice belonging to the C3H breed. They obtained a fivefold increase in myogenesis of mononucleated cells (satellite cells) following a crush injury on the mice's thighs. After 70 hours from the injury cultures were set up from the excised cells and gave rise to the C2 cell line (so called, to differentiate it from the C1 cell line, originated from cells excised 48h after the crush injury).

From this line, Blau *et al.* (1985) produced a diploid sub clone that they called C2C12, and that showed an ability to differentiate rapidly and produce contracting myotubes expressing characteristic muscle proteins.

A versatile pure population of myogenic cells was therefore established.

The literature shows contrasting opinions about whether C2C12 are a suitable cell line to develop models of muscle function.

In their respective studies, Muses, Morgan and Wells (2011) and Grabowska *et al.* (2011) warn that C2C12 use as a model remains limited to in vitro based experiments, as it has a tendency to generate tumours when transplanted into muscle. Furthermore, the same study by Grabowska *et al.* (2011) highlights the differences in myotube maturation and myogenic and adhesion protein expression between the cell line and primary myoblasts, in favour of the primary satellite cells.

Regarding the biophysical properties of contractile protein, instead, McMahon *et al.(*1994) support the use of C2C12, thanks to the well-organized myofibrils achieved during differentiation. The myofibrils, in turn, are constituted by fascicles of stress-bearing myofilament structures, which makes them suitable for studying sensitivity to calcium in the individual filaments. Briefly, C2C12as used in this study allowed the development of a method to measure contractile force at a given calcium concentration, which can work as both a cardiac and skeletal muscle contractile model.

More recently, Lambernd *et al.* (2012) declare that C2C12 cells are unsuitable to provide insight into insulin sensitivity, because their response to it is minimal, as it is minimal their production of GLUT4. In fact, C2C12 are mostly used to investigate differentiation, sarcomere development and myotube contraction.

Insulin-like Growth Factor 1

Insulin-like Growth Factor 1 [IGF-1] is an activator of the PI3K/Akt/mTOR pathway, by which it increases muscle hypertrophy. Through enhancement of this pathway it is also capable of actively counteract the effects of myostatin and myostatin-induced autophagy that negatively affect protein synthesis and muscle mass.

The PI3K/Akt/mTOR pathway is triggered when raised blood glucose levels induces pancreas β cells to produce insulin, which binds to its receptor [IR] on the cell membrane. The IR produces an allosteric change of its conformation in the domain internal to the cell which causes it to auto phosphorylate and recruit PI3K first, and then Akt and its downstream target mTOR. IGF-1, thanks to its conformational similarity with insulin, is able to bind to its receptor, the tyrosine kinase IGF1R, that auto phosphorylates creating a binding site for the cell membrane insulin receptor and downstream activation of the pathway.

Research into IGF-1 has exceptional relevance for the ageing population, for whom low levels of the growth factor have been associated with increased risk of fractures and body fat, both correlated to muscle atrophy, and thinning of the skin.

Several studies and controlled trials have been carried out, especially on the elderly, to investigate the effect on muscle mass of growth hormone (GH), either alone or in combination with resistance training (RT). One of the well-established and most important effects of GH is in fact the increase of IGF1 (Velloso, 2008). The results are contradictory, with some researches concluding that the combination of GH+RT increased lean body mass and decreased the ratio of fat/muscle (Rudman *et al.*, 1990, 1991). Conversely, others found that GH+RT did not present any advantage over RT+placebo (Taaffe *et al.*, 1994; Hennessey *et al.*, 2001; Lange *et al.*, 2002).

IGF-1 is only one of many ways by which the hypertrophic mTORC1 pathway can be enhanced, following PI3K/Akt activation. The latter seems to be able to happen in immediate and later fashions after muscle stimulation. To achieve a later activation, which can happen through either autocrine or paracrine events, common methods are the use of various nutrients such as amino acids or muscle growth factors such as IGF-1. The immediate response, instead, is believed to be originated from mechanical stimuli. This contraction-based activation results in phosphorylation of a different residue than the traditional IGF-1 based activation site on mTOR, Ser2448. Nevertheless, this still results in hypertrophy and the activation of most of the same effector pathways occurs.

The specific functioning of IGF-1 is thus well characterised, making it one of the best-established models of exercise mimetics. However, matters relating to the regulation of IGF-1 and its effect on glucose uptake during acute versus chronic exercise are still a matter of debate. Acute bouts of in vivo resistance exercise, a skeletal muscle hypertrophy model, have been shown to induce an increase in IGF-1, whereas aerobic exercise is widely recognised as a downregulating IGF-1 in humans. It is hard to pinpoint the extent of the effect exercise has on IGF-1 production. For example, resistance training leads to the growth factor being secreted locally, only within the muscles involved while systemic levels remain largely unaffected on the long term.

The aim of the present study is to investigate the use of IGF-1 in vitro to mimic chronic resistance training.

Exo1

Exo 1 is a rather newly discovered reversible inhibitor of exocytic pathways. In particular, it affects the trafficking between the endoplasmic reticulum [ER] and the Golgi apparatus, causing a redistribution of the vesicles back to the ER and seemingly without interfering with other organelles (Feng *et al.*, 2003). Perhaps due to its recent origin, its specific targets are still unknown, off-target side effects are possible (Feng *et al.*, 2003; Mishev, Dejonghe and Russinova, 2013; Ivanov, 2014) and its use in the specialised literature is not extensive.

There is yet to be a general consensus as to what concentration of Exo1 induces a quantifiable effect on cultured cells, and not many dose-response studies are available for the different cell lines. Abcam, that supplies Exo1, states that the half maximal inhibitory concentration [IC50] of Exo1 is 20µM, but (Chun *et al.*, 2008) have used a concentration as high as 100µM in their rat kidney cell culture experiments.

Choosing to administer the lower 20 µM concentration, we expect that Exo1 will cause a stress response by the endoplasmic reticulum.
It has been previously shown that ER stress induces the expression of insulin-like growth factor (IGF)-binding protein-1 (IGFBP-1), which negatively regulates the bioavailability of IGF-1 (Marchand *et al.*, 2006), in addition to hindering its binding to the insulin receptor (Allard and Duan, 2018). On the other hand, IGF-1 is capable of inhibiting ER stress and autophagy in rat smooth muscles in a time-dependent manner, with visible results at 24h and even more pronounced effects at 48h (Fang *et al.*, 2019).

Using Exo1 as a cell treatment, this study intends to explore the hypothesis that the drug will hamper the capacity of cells to develop hypertrophy when exposed to growth factors and exercise-mimicking stimuli.

Aims

In this study, myotubes from the immortalised murine cell line C2C12 were treated to induce metabolic changes similar to the ones occurring in in vivo exercise. The role of exosomal trafficking in the regulation of exercise metabolism was explored through addition of Exo1 to treated cells, constituting an experimental group of its own. Theoretically, inhibition of exocytosis by Exo1 should have ablated the release of myokines, thereby permitting the possibility to study the mechanistic role of “exercise factors” upon the best-established impact of exercise i.e. cellular growth. To study this, the use of insulin-like growth factor 1 [IGF-1] as a model of exercise mimetics was investigated. The outcome of treatments was then assessed by means of quantitative tools such as western blotting, and total protein/DNA ratio analysis as well as imaging implements.

Materials and methods

Cell culture

All procedures were carried out in a class II cabinet in sterile conditions unless otherwise stated. Mouse C2C12 myoblasts (ECACC, Salisbury, UK) were seeded in a T75 cell culture flask (Corning Life Sciences, Corning, NY, USA) and cultured in Dulbecco's Modified Eagle Medium (DMEM; Thermo Fisher Scientific, Massachusetts, USA) supplemented with 10% foetal bovine serum (FBS) (Sigma-Aldrich, UK), 1% penicillin-streptomycin solution, 1% amphotericin B and 1% L-Glutamine (all from Sigma-Aldrich, UK). The culture was maintained in an incubator at 37 °C with 5% CO2. The medium was replaced within 24h of seeding to remove the toxic dimethyl sulfoxide (DMSO) the cells had been frozen into. Following that, the medium was replaced every 48h using sterile serological pipettes.

Upon reaching 70% confluency, the cells were prepared to be split into 6-well plates (Nunclon™ Delta; Thermo Fisher Scientific, Massachusetts, USA).

The flask was washed twice with Hanks' Balanced Salt Solution (HBSS) (Sigma-Aldrich, UK) to remove the serum and cells were trypsinised using 2mL TrypLE™ Express Enzyme (1X) (Gibco, Thermo Fisher Scientific, Massachusetts, USA). The T75 was transferred to the incubator and a timer was started. After 2 minutes the flask was taken out of the incubator and transferred to the microscope to check for full detachment of the cells. Once the cells were fully detached, the flask was returned to the flow hood and media was added so that each of the 6-well plates they would be transferred to had 2 mL of cell suspension per well (a total of 12mL per plate). Prior to transferring the cell suspension to the plates, any cell clumps were dispersed by gentle pipetting. Finally, the plates were incubated, and the medium was changed every 2 days.

At ~90% confluency, differentiation was initiated by changing the medium to DMEM supplemented with 2% FBS, 1% penicillin-streptomycin solution, 1% amphotericin B and 1% L-Glutamine.

Experimental design

Experiments were carried out between day 5 and day 6 post-differentiation.

Each downstream cell culture experiment was composed of three experimental groups, each represented by a full 6-well plate (six replicate samples harvested per experimental group): a control plate (C), a treated plate (IGF-1) and a treated plate plus Exo1 (IGF-1 + Exo1).

IGF-1 treatment

The reagents for each plate were pre-mixed in 15mL Falcon Tubes and were prepared for each plate as follows:

- C :12mL DMEM (2% FBS) + 24µL DMSO
- IGF-1: 12mL DMEM (2% FBS) + 12µL IGF-1 (10ng/mL final concentration) + 24µL DMSO
- IGF-1 + Exo1: 12mL DMEM (2% FBS) + 12µL IGF-1 (10ng/mL final concentration) + 24µL Exo1 (20µM final concentration)

The reagents were transferred to the respective plates, analogously to a media change (For the preparation of IGF-1 in PBS see Appendix 1: preparation of reagents).

All plates were placed in the incubator and the experiment run for 24 and 48h.

Harvesting

In all experiments, the initiation of the reactions in each plate was staggered so that samples could be harvested at exactly the end of the time point. One hour was left between plates, to allow time for harvesting.

Harvesting was carried out on a bench, outside of the flow hood, as sterility was not required prior to lysing the cells.

The medium was poured off and discarded. After blotting the plate on absorbent paper, cold, non-sterile 1x PBS buffer was used to wash away the remaining medium from inside the wells and, through the low temperature, inhibit metabolic processes that could degrade the sample and impact its quality. Two washes with 800µL of 1x PBS were carried out.

The plate was again blotted to remove excess PBS and, depending on the downstream analyses to be carried out, a different buffer was used to collect the sample.

For western blotting, 200µL homogenisation buffer (see appendix 1, preparation of reagents) was pipetted into each well. For Protein/DNA ratio analysis, 800µL of 0.3M NaOH was added instead.

Upon addition of the correct reagent, the cell monolayer was collected using a scraper. The suspension was transferred to a labelled Eppendorf tube (Fisher, Fair Lawn, New Jersey, USA). Each well constituted a separate sample, which was placed in ice until the end of the procedure. Eventually, the samples were manually lysed by vigorous pipetting using a p200 Finnpipette.

Samples were then frozen at -30°C.

Analysis tools

Different downstream analyses were carried out. The protocols followed for the analyses will be hereby described.

Note. An IL-6 ELISA was attempted in order to analyse the activity of the secreted myokine interleukin 6 [IL-6] in autocrine/paracrine signalling but did not produce reliable results and was therefore omitted.

Western blotting

Samples were defrosted and lysed again by pipetting with a gel loading tip for 10 times. They were spun down at maximum speed for 5min at 4°C. The supernatant was transferred to fresh labelled Eppendorfs (Fisher, Fair Lawn, New Jersey, USA). Using a Nanodrop spectrophotometer the protein content of the supernatant was measured in triplicates and an average was worked out.

A solution of 0.3-10 µg/µL protein in 3x Laemmli SDS sample buffer was prepared. If samples were not used immediately, they were stored at -30 ^{o}C until required.

Each Eppendorf lid was pierced using a small syringe to provide a breather for pressure build up during heating. Samples were heated at 95^{o}C for 5 minutes using a hot block to break disulphide bridges. They were then pulsed in a centrifuge at 4°C.

Subsequently, Bio-rad XT mops running buffer (Bio-Rad, California, USA) was used to fill both sides of a Bio-rad criterion western tank. Two Bio-Rad Criterion™ XT 12% Bis-Tris Precast Gels (Bio-Rad, California, USA) into each side of the tank. The green combs were carefully removed from each gel.

The samples in Laemmli loading buffer were vortexed for 4 seconds and, using a gel loading tip, they were carefully loaded on the gels (maximum 15µL). 3µL of Precision Plus Protein™ Kaleidoscope™ Prestained Protein Standard (Bio-Rad) were also loaded at both ends of the gel.

The tank was capped and the electrodes were connected to the power pack. The run was set up for 1hr at 200V, or just before the blue dye ran off the bottom.

During the electrophoresis, 2 liters of transfer buffer were prepared (see Appendix 1: preparation of reagents). 1 liter was chilled in the freezer.

Two pieces of blotting paper and one piece of PVDF membrane were cut per gel, following the templates provided and according to the gel dimensions. The room temperature transfer buffer was used to wet the blotting paper along with three fibre pads. The proteo-sensitive PVDF membrane first needed to be permeabilised in 100% methanol for 1 minute. It was then washed in transfer buffer and stacked together with the blotting paper and the fibre pads, so as to never allow it to dry.

After electrophoresis the gel cassette was removed and broken open double-distilled H_2O (ddH_2O) was used to rinse off excess SDS that would have otherwise hindered protein binding to the PVDF membrane. The gel was soaked in transfer buffer and place gel for 5-10min.

The chilled transfer buffer was used to fill the Bio-Rad transfer tank, and a small magnetic flea was placed at the bottom of it. The tank was placed in a box filled with ice to prevent

overheating and peaks in amperage. A freezer block was added at the back of the tank for the same reason. The box was placed on a magnetic stirrer and stirring of the buffer was started to homogenise the temperature throughout the system during the electrophoresis.

The gel sandwiches were assembled inside plastic casing plates placing the gel in direct contact with the protein-binding membrane and surrounded by blotting paper and fibre pads. Air bubbles were dispersed by running a plastic roller gently over the assembly. A clasp secured and tightened the sandwich together.

The sandwiches were placed inside the transfer tank, with the black side facing the cathode.

Transfer was initiated and set up at 100V for 45mins.

Previously prepared primary antibodies were defrosted in preparation for incubation.

Small adjustments to both running and transferring time could be operated to get a better separation or transfer according to protein size.

At the end of the electrophoresis the sandwiches were removed from the tank and the membranes collected using tweezers. To check for problems in the transfer (air bubbles, uneven loading, etc.) they were then placed in a dish and stained with Ponceau S stain (Sigma Aldrich, UK) until bands appeared.

The Ponceau stain was rinsed off by washing several times in 1x tris-buffered saline + Tween 20 (TBST) buffer (see Appendix 1: preparation of reagents). The washing approximately took 15min.

PVDF membranes were incubated in a solution of 2.5% skimmed milk powder in 1x TBST. A rocker gently agitated the membranes for 1h. This step is known as “blocking”, as milk proteins saturate all the binding sites still available on the membrane (thus not occupied by the proteins contained in the original sample). This way, potential contaminants that may be targeted by the antibodies during the following step do not affect the interpretation of results.

At the end of the incubation, the membrane was placed briefly in 1x TBST to wash away milk and avoid the contamination of the primary antibodies. While in TBST, and using the protein markers as a reference, the membranes were cut with a scalpel according to the size of the proteins recognised by the antibodies of interest.

Overnight incubation with the primary antibodies followed. The membrane segments were therefore deposited in as many plastic boxes as were the antibodies required, the boxes were filled with 15-30mL of antibody solution (1:200, antibody: 2.5%BSA in 1x TBST) and then placed on a rocker at 4^{o}C. The time of the overnight incubation varied from 12 to 20 hours, depending on the sensitivity of the antibodies, empirically determined.

The following primary antibodies were purchased from Cell Signalling Technology, Beverly, MA: pmTOR (Ser2448); peEF2 (Thr56); pAkt (Ser473); pMAPK p44-p42 (ERK 1/2 - Thr202/Tyr204); p4EBP1 (Thr37-Thr46).

The next day, the blots were removed from the fridge (4^{o}C) and the antibodies were poured into falcon tubes to be frozen at -20^{o}C for further usage.

The membranes were washed three times in 1x TBST for 5 minutes with gentle agitation, following which they were incubated for 1hr at room temperature in 2.5% Milk in 1x TBST containing HRP-conjugated secondary antibody (specific to its primary antibody, in a 1:2000

dilution) with gentle agitation. The wash step in 1x TBST was repeated and the membranes were ready for visualisation.

After mixing equal volume of Millipore HRP reagent and its buffer (Merck Millipore, USA) the blots were thoroughly covered in the reagent and incubated at room temperature for a time that varied between a few seconds and 5 minutes, depending on the strength of the primary antibodies, previously determined empirically. Eventually, the excess reagent was drained out by lightly touching the corner of the blot with absorbent paper.

The blots were sandwiched between two copier plastic sheets. The protein standards were marked on the plastic with a felt pen and the corresponding molecular weight was indicated.

The assemblies were put in a Bio-Rad Chemidoc camera (Bio-Rad, California, USA) for visualisation of the chemiluminescent signal through adjustment of the exposure time.

Finally, the blots were removed from the Chemidoc camera and placed again in TBST to be Coomassie stained. All blots were normalised against Coomassie staining

Three trays were prepared, the first containing the Coomassie solution (see Appendix 1: preparation of reagents), the second containing 50% ddH_2O + 50% methanol - to remove the excess Coomassie except from the protein bands - and the third containing ddH_2O – to terminate de-staining by washing away methanol.

The blots were transferred individually in each of the trays, in the order stated, with gentle agitation, until an effect (staining, de-staining, washing) was noticed to a satisfactory degree.

Protein/DNA ratio

The harvested samples were defrosted and heated at 37°C for 30min. For illustrative purposes these will be called Base Samples.

From every Base Sample, 20µL was transferred to a fresh Eppendorf to measure the total alkaline soluble protein content (ASP) using a Nanodrop spectrophotometer and multiplying the resulting concentration by the volume of the original base sample (800µL, see harvesting protocol above).

400µL of 1M perchloric acid (PCA, VWR Chemicals, Fontanay Sous Bois, France) was added to the Base Samples, following which they were cooled at 4°C for 10 min, vortexed and then spun in a microcentrifuge at 4°C at 5000 rpm for 5 min. Taking care not to disturb the pellet, the supernatant containing RNA was transferred to fresh Eppendorfs, appropriately labelled. A further 300µL of 0.2M PCA was added to the Base Sample pellets. They were vortexed and then spun at 4°C at 5000 rpm for 5 min. The supernatant was again removed to be transferred to the RNA Eppendorfs (total volume 1.5mL). RNA content was therefore measured with a Nanodrop spectrophotometer.

The extraction and measurement of the DNA content followed a similar procedure, whereby 1mL of 2M PCA was added to the Base Sample pellets. They were then placed in the hot block at 70°C for 60 min, vortexed and spun at 4°C at 5000 rpm for 5 min to form another pellet. The DNA-containing supernatant was transferred to appropriately labelled Eppendorfs. 300µL of 2M PCA were again added to each Base Sample, vortexed and then spun down at 4°C at 5000 rpm for 5 min. The supernatant was removed into the DNA Eppendorfs, adding up to a final volume of 1.3mL. Through the DNA measurement setting on the Nanodrop, the DNA concentration was found and multiplied by the volume (1300µL).

Three measurements were carried out in total: total alkaline soluble protein (ASP) content, RNA content, DNA content. Unfortunately, the resulting data from RNA measurement was unusable due to a technical error. The ratio between ASP and DNA, a measure of the protein synthesis per unit DNA and of cell size was worked out (Waterlow, Garlick and MILL, 1978; Brook *et al.*, 2016).

Myotube diameter measurement

Picture taking method

IGF-1 was expected to enhance hypertrophic pathways, so cells were photographed at the end of the treatment just before having samples collected:

Every experiment consisted of a control, a treatment and a treatment+Exo1 plate. Each plate consisted of 6 wells. Following a similar method to the ones previously published (Stevenson *et al.*, 2005; Trendelenburg *et al.*, 2009; Bajaj *et al.*, 2011; Hughes *et al.*, 2016; Passey *et al.*, 2016; Ono and Sakamoto, 2017). A picture was taken for each of three random points, in each of the six wells, in each plate, in each experiment.

A schematic representation follows:

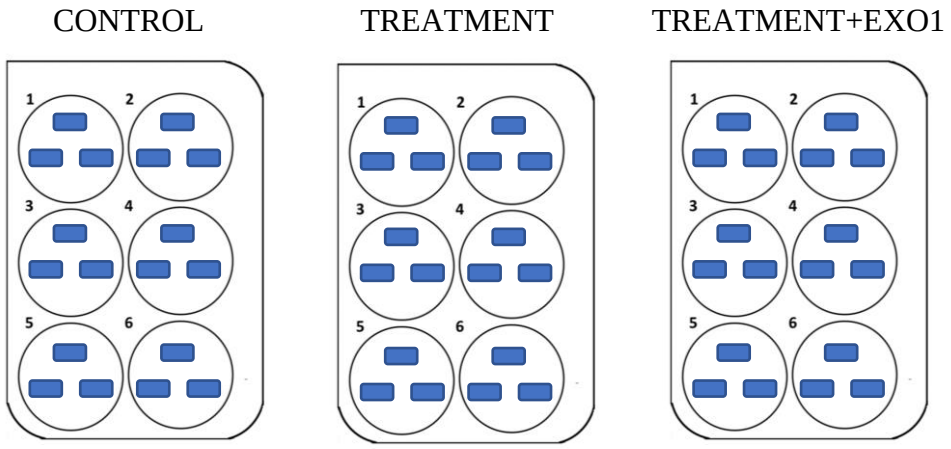


Figure 2 picture taking method. Each blue rectangle represents the area in which a picture was taken.

Wells were conventionally numbered starting with the right angle of the plate on the top left corner and its corresponding well numbered 1. Enumeration continued from left to right and down, as shown above. The digital device used is a Nikon Digital sight DS – L2 monitor, connected to a Nikon DS – Fi1 camera, mounted on a Nikon TMS – F inverted microscope. The focus used was kept constant (10X) and was reported on each image, together with the plate and well designation, through the digital tools of the DS – L2 monitor. The pictures were then used in conjunction with the open source digital image processing program ImageJ to measure myotube width. All images were saved, unmodified in TIFF format prior to processing. Additionally, a picture of a microscopic graticule was taken to set the scale of digital measurements and validate them.

Digital measurement method

The free open source image processing software ImageJ was used to measure the average width of myotubes from the pictures taken from every treatment. All images were taken using a 10x focus and saved in TIFF format. The 10x focus picture of the graticule was used to set the scale for all subsequent measurements in imageJ. By measuring the graticule length, it was established that all pictures taken with the 10x focus would have a scale of 20,330 pixels/centimetre. The scale needed to be manually reset, using always the same parameters, at every new session. Once the scale was set, a myotube image was open and a total of 20 myotubes per picture (therefore 60 myotubes per well and 360 per treatment) were considered. The method for the measurement of the average width of each myotube is hereby

described. Once a suitable myotube was identified, the measuring tool of the software was selected. The pointer was set at one point of the external silhouette of the myotube and dragged towards the opposite side of the myotube. Due to each myotube in the same picture having a different optimal focus, the silhouettes could present varying thicknesses. It was established that the middle point of the silhouette would be visually determined and would constitute the extreme point of the segments measured. Three equidistant segments were measured per myotube (at approximately the extremes and the middle of the myotube, as shown below).

ImageJ was set up to report area, mean, min, max, angle and length from the measurement taken, each showing nine decimal digits. The length was used in subsequent calculations. After each measurement, the corresponding segment was drawn onto the picture to avoid repeated measures at the same point. An average per myotube and then an average per treatment was calculated using Microsoft Excel.

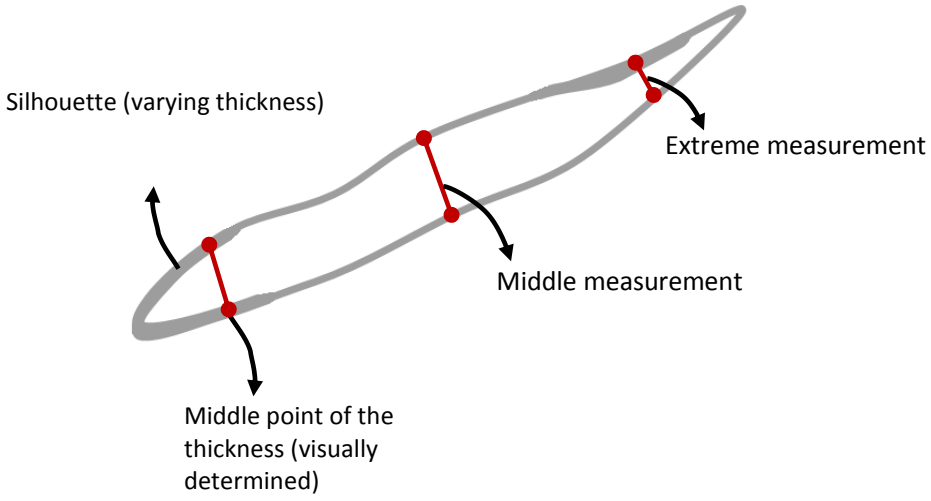


Figure 3 digital measurement method for every myotube.

Statistical analysis

The results collected were analysed through the statistical software IBM SPSS Statistics 24 (IBM, 2016).

First, the assumptions for a two-way ANOVA were tested, that's to say independent observations (which applies to our case, as every single value relates to a different sample) normal distribution of the samples populations (tested by running descriptive statistics and only considering acceptable values of skewness and kurtosis between +2 and -2, as recommended by (Gravetter and Wallnau, 2016)) and homogeneity of variances, verified with Levene's test (Pagano, 2012; De Muth, 2014; Gravetter and Wallnau, 2016).

Where such assumptions were not met, data was transformed. Skewed data were square rooted, while data with heterogeneous variances were analysed again in STATA (StataCorp, 2017) with a robust two-way ANOVA.

Secondly, the two-way ANOVA analysis was run to assess statistical differences between experimental groups. The following comparisons were therefore analysed: Control vs. IGF-1; Control vs. IGF-1+EXO1; IGF-1 vs. IGF-1+EXO1.

The graphs this way produced displayed error bars representing the standard deviation (SD).

Estimated marginal means were also plotted to better show any interactions between effects of treatment and time point and can be viewed in Appendix 3. The choice of representing the standard deviation over the standard error of the mean (SEM) is because SEM is a special type of SD (Jaykaran, 2010; Pyrczak, 2016). That is to say SD represents the spread of samples around the population mean, or the variability within a sample, whereas SEM represents the possible variability of the mean itself (De Muth, 2014). Knowing the SD (σ) and sample size(n), computing the SEM is a straightforward task (Pyrczak, 2016)

$$SEM = \frac{\sigma}{\sqrt{n}}$$

In the bar charts reported below, an outcome was considered significantly different when the p value was below 0.05 and was thus indicated with lines connecting two bars.

Results

Hereby reported is an overview of the effect of IGF-1±Exo1 treatment on myotube width. Subsequently, a deeper insight will be given by the results of the western blots carried out upon harvesting C2C12 cells after the interventions. The section will be arranged following the pathway of activation of mTOR and proceeding down to its downstream targets.
It will then terminate with an analysis of the total protein and DNA ratio produced as a consequence of the treatment.

Results in the bar charts are expressed as mean ± SD and clustered according to the time point. Lines connecting two bars represent a significant difference ($p<0.05$).

Western blot results are expressed in relative arbitrary units relating to band intensity.

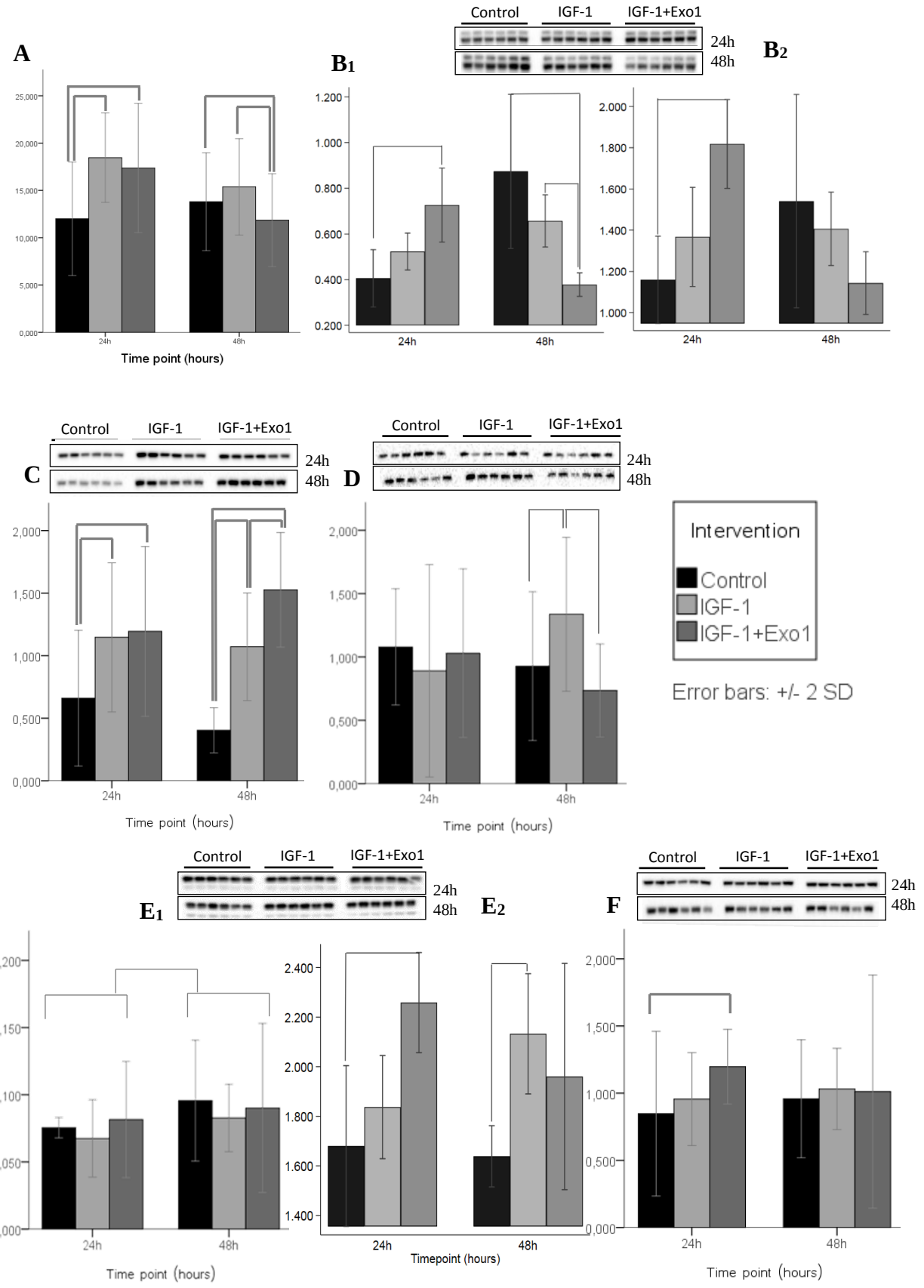


Figure 4. Digital analysis of the myotube width following IGF-1±Exo1 treatment [A]. Western blotting, expression of pMAPK_p44/Erk1 [B_1] and pMAPK_p42/Erk2 [B_2], Akt phosphorylation at Ser473 [C], mTOR phosphorylation at Ser4228 [D], expression of p4EBP1-15kDa [E_1] and p4EBP1-20kDa [E_2] expression of pEEF2 (Thr56) [F].

Myotube width is increased at 24h in both treated groups and is decreased at 48h by Exo1 addition.

Figure 3A shows that a significant hypertrophic phenotype is visible already after 24h of IGF-1 treatment but such effect is blunted after 48h.
After 24h IGF-1+Exo1 treatment, myotubes are significantly wider than the control, but do not display a decrease from the IGF-1 group. Figure 3B shows how this trend is inverted in the longer time point, with IGF+Exo1 cells resulting significantly thinner than both other groups.

Exo1 increases pMAPK-Erk1/2 (Thr202/Tyr204 and Thr185/Tyr187) phosphorylation at 24h but decreases it at 48h.

The phosphorylation of both Erk1 and Erk2 is substantially upregulated at 24h in presence of Exo1 (Figure $3B_1$ and B_2). At 48h, instead, the situation is entirely inverted and Exo1 heavily decreases the amount of phosphorylated Erk1. The estimated marginal means plots (Figure $5A_1$ and A_2) suggest that a similar trend could be delineated for Erk2 as well but the great variability in the control group impedes a clearer picture of the situation at 48h.
Neither isoform is affected by IGF-1 treatment.

Akt phosphorylation at Ser473 is increased by IGF-1 and boosted by Exo1.

In Figure 3C, at both time points, pAkt shows a clear and significant increase thanks to the addition of IGF-1. Exo1 too causes an increase at 24h and even increases phosphorylation of Akt at 48h, compared to the IGF-1 treatment.

As visible in Figure 5B, the intervention has a significant main effect, because the trend whereby IGF-1 produces a higher amount of pAkt and the addition of Exo1 amplifies its effect (to some extent) is conserved throughout the time points. It must be noted, however, that Exo-1 does not produce a significant difference compared to the IGF-1 group at 24 hours (see Figure 5B).

PmTOR (Ser4228) is upregulated by IGF-1 at 48h and downregulated by Exo1.

Figure 3D shows how the treatment doesn't elicit any effect after 24h, but the 48h intervention displays the expected increase in pmTOR in the IGF-1 group.
Addition of the ER-Golgi crosstalk inhibitor brings pmTOR back to control levels (Figure 6B).

Exo1 affects 4EBP1 phosphorylation at Thr37/46 at 24h, while IGF-1 only affects it at 48h.

In figure 7D, p4EBP1 20kDa is unaffected by IGF-1 treatment until the 48h time point, after which it is increased.
Exo1 greatly upregulates p4EBP1 20kDa at 24h but at 48h the large variability within the group (See Figure 7D) shows the effect is not conserved for the longer time point.
p4EBP1 15kDa is unaffected by either treatments (Figure 7B).

Exo1 increases phosphorylation of eEF2 (Thr56) at 24h

Rather surprisingly, peEF2 Thr56, usually an indicator of atrophy, is not decreased by the presence of IGF-1 at either time point (Figure 8B).
Addition of Exo1increases peEF2 at 24h, while the 48h treatment group remains unaffected (Figure 8B).

IGF-1 treatment increases ASP per DNA unit at 48h. Exo1 addition increases dsDNA at 24h and boosts protein synthesis per DNA unit at 48h.

Table 1shows the results of total protein, total DNA and protein/DNA ratio analysis. Graphed results, including bar charts and predictive marginal means are included in Appendix 2.

All results below are expressed in the specified units (protein - mg, DNA - µg, protein/DNA - µg/µg) plus or minus the standard deviation.

	Time point	Control	IGF-1	IGF-1 + Exo1	IGF-1 vs Control	IGF-1 vs IGF-1+Exo1	Control vs IGF-1+Exo1
Total protein (mg)	24h	1.070 ± 0.358	1.197 ± 0.284	1.007 ± 0. 092	*P*= 0.363	*P*= 0.176	*P*= 0.648
	48h	1.402 ± 0.131	2.094 ± 0.176	1.896 ± 0.131	*P*= 0.000*	*P*= 0.159	*P*= 0.001*
Total dsDNA (µg)	24h	26.325 ± 3.528	27.193 ± 1.342	29.817 ± 3.304	*P*= 0.592	*P*= 0.112	*P*= 0.037*
	48h	20.186 ± 2.002	23.133 ± 1.497	17.846 ± 2.660	*P*= 0.076	*P*= 0.002*	*P*= 0.154
Protein/DNA (µg/µg)	24h	41.318 ±14.160	43.923 ±9.618	33.985 ±3.471	*P*= 0.999	*P*= 0.714	*P*= 0.897
	48h	69.547 ±3.070	91.104 ±11.416	108.455 ±16.982	*P*= 0.045*	*P*= 0.162	*P*= 0.000*

Table 1Total protein, total DNA and protein/DNA ratio analysis. Results are expressed as mean ± SD. Asterisks indicate a significant difference ($p<0.05$)

Table 1 shows that, while the protein/DNA analysis of the 24h IGF-1 experiment does not show any significant difference, the effects are instead clearly visible in the 48h analysis whereby the total protein as well as the ASP:DNA ratio are increased.

At 24h Exo1 only increases total dsDNA compared to the Control group.
At 48h, instead, it increases total ASP, similarly to IGF-1. dsDNA sees a decrease compared to IGF-1 and drops back at control levels. ASP/DNA is boosted, again following IGF-1.

Discussion

This chapter aims at characterising the response of well-established markers of hypertrophy to IGF-1 treatment in C2C12 cells. This research proposes the in-vitro study of such response as a model for research into the metabolic effects of in vivo exercise.

Further insight into the role of ER-Golgi crosstalk on the regulation of said markers is given by the addition of Exo-1, a molecule whose proposed function is to disrupt vesicular trafficking from the endoplasmic reticulum without disturbing other organelles.

The table below summarises the main findings from both treatments.

	Result
IGF-1	IGF-1 increased myotube width at 24h
	IGF-1 elicited mTORC2 at 24h, followed by mTORC1 at 48h.
	IGF-1 triggered hypertrophy independently from pMAPK
IGF-1+Exo1	Exo1 induced ER stress, as shown by an increase in pEEF2 at 24h
	IGF-1 overcompensated for ER stress by inducing hypertrophy at 24h, but the effect was blunted after 48h.
	Hypertrophy was achieved by phosphorylation of ERK1/2 and pAkt

Table 2Main findings from IGF-1 and IGF-1+Exo1 treatment of C2C12 cells for 24 and 48h.

IGF-1 treatment enhances hypertrophy at the earlier 24h time point through activation of mTORC2 and follows up with mTORC1 at 48h.

Previous studies report that the average width of 6 days post-differentiation C2C12 myotubes (considering our experiments were initiated between day 5 and 6) is about 20µm (Ono and Sakamoto, 2017). In this experiment, control cells reached an average 12.0µm after 24h and 13.8µm after 48h. After addition of IGF-1, 24h and 48h treated cells average 18.5µm and 15.3µm in width, respectively. 24h treated cells exhibited a 54.2% increase, while 48h treated cells did not grow significantly and only displayed an 11.6% increase compared to their corresponding control group. Measuring myotube width is an indicator of muscle protein breakdown or synthesis, whose balance is the driving force of atrophy and hypertrophy both in vivo and in vitro (Murphy *et al.*, 2016).

Literature is abundant in studies about the pharmacokinetics of human IGF-1 or its stability for storage purposes but lacks information about its half-life in in vitro studies, especially from a mouse or rat source. In human blood, for instance, the half-life of IGF-1 is reportedly 12h (Hinson, Raven and Chew, 2007). It is worth considering the possibility that the IGF-1 drug may have degraded over the long course of the treatment, its properties might have changed and it may have lost its effect on the myotubes after 48h, giving time to the control group to further develop and level up with the treated groups. However, this does not mean that metabolic processes are unaffected after the long 48h treatment.

Given the different response of the cells after 24 or 48 hours, we asked what molecular pathways underlay this behaviour. Established markers of hypertrophy, Akt and mTOR were hence analysed, together with their upstream and downstream targets.

The hypertrophic response shown by myotubes at 24h is, in fact, explained when looking at the increase in pAkt (Ser473) levels. Evidence of this has also reported in the in vitro study by

Miyazaki and colleagues (2010), who treated C2C12 cells with IGF-1 and saw an increase in Akt Ser473 within just one hour.

Curiously, this is not mirrored by an increase in pmTOR. Akt is phosphorylated at Ser473 by mTORC2, the latter being, in turn, susceptible to activation by insulin (Wullschleger, Loewith and Hall, 2006; Cybulski *et al.*, 2009). It has been shown in vivo studies that during acute resistance training (RT) hypertrophy can be triggered by both rapamycin-sensitive mTOR-dependent and -independent pathways (Ogasawara *et al.*, 2016). Essentially, both mTORC1 (rapamycin-sensitive) and mTORC2 (rapamycin-insensitive) activation can result in hypertrophy. Their results show that after just 1h post RT the levels of pAkt (Ser473) increased, irrespective of rapamycin administration.
This evidence is in accordance with the present study and may implicate that in this case mTORC2 was activated and caused hypertrophy at 24h. While this continued over the 48h period (with pAkt Ser473 still steeply increasing), the longer time point may have also triggered mTORC1, as suggested by the increase of mTOR Ser4228. It is unclear, though, why this does not result in 48h treated myotubes being significantly larger than the control.

It is possible that in a chronic model of in vivo RT, and particularly in a fed state (to elicit insulin release) the behaviour of mTORC2 is similar. The latter is in fact implicated in insulin sensitivity as well as glucose uptake, depending on its localisation in the cell (Hodson *et al.*, 2017).

IGF-1 could therefore be used as a tool to examine the effects of mTORC2 localisation on hypertrophy.

The increase in width at 24h is in apparent antithesis with the expression of ERK1 and ERK2. Strikingly, the 24h IGF-1 group does not significantly differ from the control. In fact, the MAPK cascade is known to be triggered by IGF-1 (Hakuno and Takahashi, 2018) but Milasincic and colleagues (1996) hint at the existence of a possible IGF-1-induced, MAP kinase-independent signalling event which contributes to the myogenic response of the growth factor in C2C12 cells. In their experiment, it appears that IGF-1 is able to initiate a growth response in both a MAP kinase dependent and a MAP kinase-independent manner. Their cells were also administered a MAPK inhibitor, but still displayed a myogenic effect. Evidently, the same conditions for MAPK-independent hypertrophy were not verified upon the 48h time point, whereby neither pMAPK p42/p44 nor myotube width are increased.

This is an interesting point for further study: if IGF-1 alone is able to induce the ERK pathway, even when its kinase is hindered by a mutation or an inhibitor (Rauch *et al.*, 2011) it should shed light on localised, rather than systemic effects of resistance training-induced IGF-1 production. It was observed, in fact, that COPD patients (who often experience muscle fibre thinning and even cachexia) can see their quadriceps muscle synthesis improved by resistance training by means of an increase in the local expression of IGF-1

Unexpectedly, peEF2 Thr56 is unchanged by IGF-1 treatment at either time point. eEF2 is thought to be regulated by insulin through mTORC1 (Browne and Proud, 2004). Because pmTOR Ser4228 too is unaffected at 24h this may partially explain the behaviour of peEF Thr56. However, it is insufficient to justify it at 48h. The literature reports that mTORC2 is inhibited by mTORC1 by means of a negative feedback loop that involves S6K1phosphorylating insulin receptor substrate and thus impairing the insulin-P13K-Akt pathway (Showkat, Beigh and Andrabi, 2014). As mentioned earlier, this kinase

dephosphorylates eEF2. If, however, mTORC1 has been triggered by 48h, then this has potentially activated the negative feedback loop, resulting in peEF2 not decreasing. It is likely, though, that the time point observed is only representative of the beginning of said feedback: in fact, this would implicate a net increase in peEF2 and a decrease in pmTOR Ser4228, which these results do not show yet. The analysis of a further time point may help clarify whether this is the case.

It has been previously observed in an in vivo mouse model that chronic resistance training does not increase the phosphorylation of p4EBP1 Thr37/46, and could even blunt other markers of hypertrophy downstream of mTOR (Ogasawara *et al.*, 2013). In the same study, Ogasawara and colleagues found that, while a short period of detraining could restore the levels of phosphorylation of the other markers, p4EPB1 remained unchanged. If, on the one hand, Barazzoni *et al.* (2012) found that insulin had no effect on 4EBP1 phosphorylation, amino acid availability being the limiting factor, it is also true, on the other hand, that in abundance of amino acids insulin is able to transiently or permanently increase phosphorylation of 4EBP1 in various types of cells, among which smooth muscle cells (Terruzzi, Pellegatta and Luzi, 2005). Even more surprising is, therefore, the upregulation of the 20kDa residue at 48h, considering that most of the amino acids in the media should have been used up and that it is not associated to an increase in p4EBP1 15kDa. Despite this, pmTOR may have played a role in p4EBP1 20kDa phosphorylation, given that the two are both unchanged at 24h, while increasing at 48h.
The discrepancy between the expressions of the two subunits would be an interesting point for further research.

Although myotube width analysis shows an increase in hypertrophy after 24h in the IGF-1 treated group data about total protein, DNA and protein/DNA show no effect of the treatment at 24h.
Meanwhile, the longer time point indicates that the treated groups have a higher rate of protein synthesis per DNA unit. Once more, though, this result is not supported by the myotube width data: this raises the question whether it is possible that the proteins produced are not intended to increase cell size, but to support the internal metabolic processes stimulated by the treatments.

ER stress induced by IGF-1+Exo1 elicits hypertrophy at 24h, but the effect is blunted after 48h.

After 24h IGF-1+Exo1 treatment, myotubes are 45% wider than the control (average 17.4µm), but do not display a significant decrease from the IGF-1 group. However, when IGF-1 addition does not yield any significant growth compared to the control at 48h, IGF+Exo1 cells exhibit the expected atrophic trend, with myotubes resulting significantly thinner than their IGF-1 counterparts (-22.7%, average 119µm) as well as the control (-13.8%).

The pattern of pMAPK in IGF-1 + Exo1 treated cells mirrors that of the myotube width. With the ER trafficking inhibitor enhancing phosphorylation of both ERK1 and ERK2, suggesting increased protein synthesis. This does not appear to be due to an intense hypertrophic effect by IGF-1 counteracting the negative effects that Exo1 has on the ER, because the IGF-1 group is not different from the control, as pointed out above. It is possible, however, that a drug to drug interaction has created the hypertrophic effect.

After 48h, the steep increase in both pMAPK isoforms verified at 24h may have been dampened by a negative feedback loop in which ERK can inhibit its own activators, among which Raf and MEK (Mendoza, Er and Blenis, 2011). To confirm this, it would be interesting to measure the behaviour of said markers under the conditions of this study.

Once again, pAkt post-24h IGF-1+Exo1 treatment suggests an activation of hypertrophy, but it does not differ from the IGF-1 group. Then, even more unexpectedly, the effect is not only conserved, but enhanced at 48h, where phosphorylation of pAkt Ser473 is boosted significantly more than in the IGF-1 group.

In contrast, the pmTOR result remains unchanged at 24h, but the significant upregulation triggered by IGF-1 at 48h is promptly inhibited by Exo1, which takes the rapamycin-sensitive marker of hypertrophy back to control levels.

Activation of pmTOR Ser2448 is in fact independent from pAkt Ser473 (Chiang and Abraham, 2005). In order to better understand the behaviour of mTOR, it would be interesting to look at the expression of p70S6K, its downstream target. Like in the case of IGF-1 treatment alone, the results of pAkt Ser473 and pmTOR Ser 4228 may once again indicate an activation of mTORC2-driven hypertrophy at 24h, mTORC2 complex being the putative pAkt Ser473 kinase (Chen *et al.*, 2013).

Although hypertrophy may be occurring in presence of Exo1, the compound still seems to put strain on the endoplasmic reticulum, as shown by a 24h pEEF2 increase. Such increase in the phosphorylation, therefore deactivation of eEF2 (a marker of protein elongation during synthesis) at Thr56 has been previously linked to stress, nutrient deprivation and bacterial infection (Frost, Pereyra and Lang, 2011). Phosphorylation of EEF2 eventually drops back to control levels at 48h.

Throughout the literature, different effects of endoplasmic reticulum stress have been reported, and are only apparently contradictive. On the one hand, impaired function of the endoplasmic reticulum activates the unfolded protein response (UPR), whose downstream signalling plays a role in both restoring ER function and myogenesis (Sun *et al.*, 2013). A relationship has even been proposed with IGF-1, this latter being partly responsible for the activation of said restorative pathways (Novosyadlyy *et al.*, 2008).

On the other hand, anabolic resistance given by a decreased sensitivity to amino acids as a consequence of UPR may block the hypertrophic mTORC1 pathway (Deldicque *et al.*, 2011).

Because the IGF+Exo1 experiment does not show evidence of mTORC1 activation, the possibility is still open that the hypertrophy verified at 24h may be due to mTORC2.

At 24h this may have induced the myotube hypertrophy, while at 48h, anabolic resistance may have taken over and not only prevented any measurable increase in the myotube width, but actually promoted a distinct atrophic phenotype. Deldicque and colleagues (2011) have already demonstrated how anabolic resistance can be induced in C2C12 in as little as 17h treatment with chemical inducers of ER stress, even though the short time point they used was insufficient to prevent insulin from stimulating protein synthesis.

Collectively, these results seem to hint at an activation of hypertrophy in IGF-1+Exo1 treated cells at 24h, contrarily to expectations for which an impaired ER-Golgi crosstalk should have promoted atrophy. Perhaps such increase in hypertrophy is due to an attempt to overcompensate for ER stress, as previously mentioned. If so, the combination of IGF-1 and Exo1 could be a useful tool to investigate pathologies related to protein misfolding caused by mutations in the ER (Lin, Walter and Yen, 2008) and IGF-1 could be a research target for the treatment of ER stress-induced pathologies.

However, the yield at 48h points to a more atrophic effect. It is unclear, though, where the striking upregulation of pAkt at the latter time point fits into the picture

While DNA concentration remains unchanged throughout the treatments at 24h, addition of Exo1 slightly decreases it after 48h, compared to the IGF-1 group. The protein synthesis per unit DNA is instead boosted.

Conclusion

IGF-1 presents different responses at 24h and 48h.

At 24h myotube width is increased as shown by a steep increase in pAkt Ser473, in accordance with previous studies. pmTOR Ser4228 is unaffected at this time point, which suggests mTORC2, as opposed to mTORC1 may be responsible for the activation of Akt and subsequent hypertrophic response. The latter shows to be independent of MAPK signalling. mTORC1 is instead activated and 48h.

Exo1 addition to IGF-1 the treatment elicits ER stress, which is overcompensated for by IGF-1 enhancing hypertrophy. The effect is then lost at 48 hours.

Based on these findings we conclude that IGF-1 could be used as a tool to investigate some aspects of in vivo resistance training such as the effect of mTORC2 cellular localisation on hypertrophy and the local outcome over RT-induced IGF-1 on muscles. These findings are relevant to the ageing population, as well as carriers of pathologies like COPD-related cachexia and diseases that involve an impaired Golgi-ER crosstalk.

Future research should be aimed at a further characterisation of the effects of Exo1, to be able to investigate the behaviour of mTORC1 and its downstream pathways under the same conditions, or at longer timepoints.

References

Allard, J. B. and Duan, C. (2018) 'IGF-binding proteins: Why do they exist and why are there so many?', *Frontiers in endocrinology*. Frontiers, 9, p. 117.

Bajaj, P. *et al.* (2011) 'Patterning the differentiation of C2C12 skeletal myoblasts', *Integrative Biology*, 3(9), pp. 897–909.

Barazzoni, R. *et al.* (2012) 'Insulin fails to enhance mTOR phosphorylation, mitochondrial protein synthesis, and ATP production in human skeletal muscle without amino acid replacement', *American Journal of Physiology-Endocrinology and Metabolism*, 303(9), pp. E1117–E1125.

Barbieri, E. *et al.* (2011) 'Morphofunctional and Biochemical Approaches for Studying Mitochondrial Changes during Myoblasts Differentiation', *J Aging Res*. Department of Biomolecular Sciences, University of Urbino Carlo Bo, Via I Maggetti, 26, 61029 Urbino (PU), Italy., 2011, p. 845379. doi: 10.4061/2011/845379.

Barone, V. *et al.* (2015) 'Yip1B isoform is localized at ER–Golgi intermediate and cis-Golgi compartments and is not required for maintenance of the Golgi structure in skeletal muscle', *Histochemistry and cell biology*. Springer, 143(3), pp. 235–243.

Barreiro, E. and Gea, J. (2016) 'Amino Acid and Protein Metabolism in Pulmonary Diseases and Nutritional Abnormalities: A Special Focus on Chronic Obstructive Pulmonary Disease', in *The Molecular Nutrition of Amino Acids and Proteins*. Elsevier, pp. 145–159.

Blau, H. M. *et al.* (1985) 'Plasticity of the differentiated state', *Science*, 230(4727), pp. 758–766.

Booth, F. W. and Laye, M. J. (2009) 'Lack of adequate appreciation of physical exercise's complexities can pre-empt appropriate design and interpretation in scientific discovery', *The Journal of physiology*, 587(23), pp. 5527–5539.

Borer, K. T. (2005) 'Physical activity in the prevention and amelioration of osteoporosis in women', *Sports medicine*, 35(9), pp. 779–830.

Boulinguiez, A. *et al.* (2017) 'Mitochondria and endoplasmic reticulum: Targets for a better insulin sensitivity in skeletal muscle?', *Biochimica et Biophysica Acta (BBA)-Molecular and Cell Biology of Lipids*, 1862(9), pp. 901–916.

Brook, M. S. *et al.* (2016) 'Synchronous deficits in cumulative muscle protein synthesis and ribosomal biogenesis underlie age-related anabolic resistance to exercise in humans', *The Journal of physiology*, 594(24), pp. 7399–7417. Available at: https://www.ncbi.nlm.nih.gov/pmc/articles/PMC5157077/pdf/TJP-594-7399.pdf.

Browne, G. J. and Proud, C. G. (2004) 'A novel mTOR-regulated phosphorylation site in elongation factor 2 kinase modulates the activity of the kinase and its binding to calmodulin', *Molecular and cellular biology*. Am Soc Microbiol, 24(7), pp. 2986–2997.

Chen, S. *et al.* (2013) 'IBP-mediated suppression of autophagy promotes growth and metastasis of breast cancer cells via activating mTORC2/Akt/FOXO3a signaling pathway', *Cell death & disease*. Nature Publishing Group, 4(10), p. e842.

Chen, Y.-W., Barberio, M. D. and Hubal, M. J. (2016) 'Genes in Skeletal Muscle Remodeling and Impact of Feeding: Molecular and Cellular Aspects', in *The Molecular Nutrition of Amino Acids and Proteins*. Elsevier, pp. 315–329.

Chiang, G. G. and Abraham, R. T. (2005) 'Phosphorylation of mammalian target of rapamycin (mTOR) at Ser-2448 is mediated by p70S6 kinase', *Journal of Biological Chemistry*, 280(27), pp. 25485–25490. Available at: http://www.jbc.org/content/280/27/25485.full.pdf.

Chun, J. *et al.* (2008) 'Characterization of class I and II ADP-ribosylation factors (Arfs) in live cells: GDP-bound class II Arfs associate with the ER-Golgi intermediate compartment independently of GBF1', *Molecular biology of the cell*, 19(8), pp. 3488–3500. Available at: https://www.ncbi.nlm.nih.gov/pmc/articles/PMC2488303/pdf/zmk3488.pdf.

Cooper, G. M. (2000) 'Actin, myosin, and cell movement', *The Cell: a molecular approach*.

Cybulski, N. *et al.* (2009) 'mTOR complex 2 in adipose tissue negatively controls whole-body growth', *Proceedings of the National Academy of Sciences*. National Acad Sciences, 106(24), pp. 9902–9907.

Das, A. K. *et al.* (2012) 'AMP-activated protein kinase stimulates myostatin expression in C2C12 cells', *Biochem Biophys Res Commun*. Department of Animal Sciences, Washington State University, Pullman, WA 99164, USA., 427(1), pp. 36–40. doi: 10.1016/j.bbrc.2012.08.138.

Deldicque, L. *et al.* (2011) 'ER stress induces anabolic resistance in muscle cells through PKB-induced blockade of mTORC1', *PloS one*. Public Library of Science, 6(6), p. e20993.

Dillon, E. L. (2016) 'Protein Metabolism in the Elderly: Molecular and Cellular Aspects', *The Molecular Nutrition of Amino Acids and Proteins: A Volume in the Molecular Nutrition Series*.

Egawa, T. *et al.* (2014) 'AICAR-induced activation of AMPK negatively regulates myotube hypertrophy through the HSP72-mediated pathway in C 2 C 12 skeletal muscle cells', *American Journal of Physiology-Endocrinology and Metabolism*, 306(3), pp. E344–E354.

English, A. R. and Voeltz, G. K. (2013) 'Endoplasmic reticulum structure and interconnections with other organelles', *Cold Spring Harbor perspectives in biology*. Cold Spring Harbor Lab, 5(4), p. a013227.

Evers-van Gogh, I. J. *et al.* (2015) 'Electric Pulse Stimulation of Myotubes as an In Vitro Exercise Model: Cell-Mediated and Non-Cell-Mediated Effects', *Sci Rep*. Molecular Cancer Research and Center for Molecular Medicine, University Medical Centre Utrecht, Universiteitsweg 100, 3584 CG, Utrecht, The Netherlands. Nutrition, Metabolism and Genomics Group, Division of Human Nutrition, Wageningen University, PO BOX 8, 5, p. 10944. doi: 10.1038/srep10944.

Fan, W. and Evans, R. M. (2017) 'Exercise mimetics: impact on health and performance', *Cell metabolism*, 25(2), pp. 242–247.

Fang, X. *et al.* (2019) 'Effects of insulin-like growth factor-1 on endoplasmic reticulum stress and autophagy in rat gastric smooth muscle cells cultured at different glucose concentrations in vitro', *Molecular and cellular biochemistry*. Springer, 451(1–2), pp. 11–20.

Feng, Y. *et al.* (2003) 'Exo1: a new chemical inhibitor of the exocytic pathway', *Proc Natl Acad Sci U S A*. Institute of Chemistry and Cell Biology, Department of Cell Biology, Harvard Medical School, Boston, MA 02115, USA. yfeng@hms.harvard.edu, 100(11), pp. 6469–6474. doi: 10.1073/pnas.0631766100.

Frost, R. A., Pereyra, E. and Lang, C. H. (2011) 'Ethyl pyruvate preserves IGF-I sensitivity toward mTOR substrates and protein synthesis in C2C12 myotubes', *Endocrinology*, 152(1), pp. 151–163.

Goodyear, L. J. (2008) 'The exercise pill—too good to be true?', *New England Journal of Medicine*, 359(17), pp. 1842–1844.

Grabowska, I. *et al.* (2011) 'Comparison of satellite cell-derived myoblasts and C2C12 differentiation in two-and three-dimensional cultures: changes in adhesion protein expression', *Cell biology international*, 35(2), pp. 125–133. Available at: http://onlinelibrary.wiley.com/store/10.1042/CBI20090335/asset/CBI20090335.pdf?v=1&t=jal6ahi5&s=7130aa48646a6dbfc1a05f314e4a37f6f503aa3d.

Gravetter, F. J. and Wallnau, L. B. (2016) *Statistics for the behavioral sciences*. Cengage Learning.

Guerrieri, D., Moon, H. Y. and van Praag, H. (2017) 'Exercise in a Pill: The Latest on Exercise-Mimetics', *Brain Plasticity*, 2(2), pp. 153–169.

Hakuno, F. and Takahashi, S.-I. (2018) '40 YEARS OF IGF1: IGF1 receptor signaling pathways', *Journal of Molecular Endocrinology*, 61(1), pp. T69–T86. doi: 10.1530/jme-17-0311.

Handschin, C. (2016) 'Caloric restriction and exercise "mimetics"': Ready for prime time?"', *Pharmacol Res*. Biozentrum, University of Basel, Klingelbergstrasse 50/70, CH-4056 Basel, Switzerland. Electronic address: christoph.handschin@unibas.ch., 103, pp. 158–166. doi: 10.1016/j.phrs.2015.11.009.

Hennessey, J. V *et al.* (2001) 'Growth hormone administration and exercise effects on muscle fiber type and diameter in moderately frail older people', *Journal of the American Geriatrics Society*. Wiley Online Library, 49(7), pp. 852–858.

Hinson, J., Raven, P. and Chew, S. L. (2007) *The endocrine system*. Elsevier Health Sciences.

Hodson, N. *et al.* (2017) 'Differential localization and anabolic responsiveness of mTOR complexes in human skeletal muscle in response to feeding and exercise', *American Journal of Physiology-Cell Physiology*. American Physiological Society Bethesda, MD, 313(6), pp. C604–C611.

Hughes, D. C. *et al.* (2016) 'Testosterone enables growth and hypertrophy in fusion impaired myoblasts that display myotube atrophy: deciphering the role of androgen and IGF-I receptors', *Biogerontology*, 17(3), pp. 619–639.

IBM (2016) 'SPSS statistics for Windows'. Edited by I. B. M. Corp. New York.

Ivanov, A. I. (2014) 'Pharmacological inhibitors of exocytosis and endocytosis: novel bullets for old targets', *Exocytosis and Endocytosis*, pp. 3–18. Available at: https://www.researchgate.net/profile/Andrei_Ivanov4/publication/263292675_Pharmacological_Inhibitors_of_Exocytosis_and_Endocytosis_Novel_Bullets_for_Old_Targets/links/53dfd8150cf2a768e49bed3b.pdf.

Jaykaran, J. (2010) '" Mean±SEM" or" Mean (SD)"?'

Kanzleiter, T. *et al.* (2014) 'The myokine decorin is regulated by contraction and involved in muscle hypertrophy', *Biochemical and biophysical research communications*, 450(2), pp. 1089–1094.

Kishioka, Y. *et al.* (2008) 'Decorin enhances the proliferation and differentiation of myogenic cells through suppressing myostatin activity', *Journal of cellular physiology*, 215(3), pp. 856–867. Available at: http://onlinelibrary.wiley.com/store/10.1002/jcp.21371/asset/21371_ftp.pdf?v=1&t=jb2qe2ir&s=e775956c724de09b8f85431613a2cec04aaa260e.

Lambernd, S. *et al.* (2012) 'Contractile activity of human skeletal muscle cells prevents insulin resistance by inhibiting pro-inflammatory signalling pathways', *Diabetologia*, 55(4), pp. 1128–1139.

Lange, K. H. W. *et al.* (2002) 'GH administration changes myosin heavy chain isoforms in skeletal muscle but does not augment muscle strength or hypertrophy, either alone or combined with resistance exercise training in healthy elderly men', *The Journal of Clinical Endocrinology & Metabolism*. Oxford University Press, 87(2), pp. 513–523.

Lin, J. H., Walter, P. and Yen, T. S. B. (2008) 'Endoplasmic reticulum stress in disease pathogenesis', *Annu. Rev. pathmechdis. Mech. Dis.* Annual Reviews, 3, pp. 399–425.

Marchand, A. *et al.* (2006) 'Endoplasmic reticulum stress induction of insulin-like growth factor-binding protein-1 involves ATF4', *Journal of Biological Chemistry*. ASBMB, 281(28), pp. 19124–19133.

McMahon, D. K. *et al.* (1994) 'C2C12 cells: biophysical, biochemical, and immunocytochemical

properties', *American Journal of Physiology - Cell Physiology*, 266(6), pp. C1795–C1802.

Mendoza, M. C., Er, E. E. and Blenis, J. (2011) 'The Ras-ERK and PI3K-mTOR pathways: cross-talk and compensation', *Trends in biochemical sciences*. Elsevier, 36(6), pp. 320–328.

Milasincic, D. J. *et al.* (1996) 'Stimulation of C2C12 myoblast growth by basic fibroblast growth factor and insulin-like growth factor 1 can occur via mitogen-activated protein kinase-dependent and-independent pathways', *Molecular and Cellular Biology*, 16(11), pp. 5964–5973.

Mishev, K., Dejonghe, W. and Russinova, E. (2013) 'Small molecules for dissecting endomembrane trafficking: a cross-systems view', *Chemistry & biology*, 20(4), pp. 475–486.

Miyazaki, M., McCarthy, J. J. and Esser, K. A. (2010) 'Insulin like growth factor-1-induced phosphorylation and altered distribution of tuberous sclerosis complex (TSC) 1/TSC2 in C2C12 myotubes', *The FEBS journal*. Wiley Online Library, 277(9), pp. 2180–2191.

Montazeri, A. (2008) 'Health-related quality of life in breast cancer patients: a bibliographic review of the literature from 1974 to 2007', *Journal of experimental & clinical cancer research*, 27(1), p. 32.

Murphy, S. M. *et al.* (2016) 'Optimization of an in vitro bioassay to monitor growth and formation of myotubes in real time', *Bioscience reports*. Portland Press Limited, 36(3), p. e00330.

Muses, S., Morgan, J. E. and Wells, D. J. (2011) 'A new extensively characterised conditionally immortal muscle cell-line for investigating therapeutic strategies in muscular dystrophies', *PloS one*, 6(9), p. e24826.

De Muth, J. E. (2014) *Basic statistics and pharmaceutical statistical applications*. Chapman and Hall/CRC.

Nocon, M. *et al.* (2008) 'Association of physical activity with all-cause and cardiovascular mortality: a systematic review and meta-analysis', *European Journal of Cardiovascular Prevention & Rehabilitation*, 15(3), pp. 239–246.

Novosyadlyy, R. *et al.* (2008) 'Insulin-like growth factor-I protects cells from ER stress-induced apoptosis via enhancement of the adaptive capacity of endoplasmic reticulum', *Cell death and differentiation*. Nature Publishing Group, 15(8), p. 1304.

Ogasawara, R. *et al.* (2013) 'mTOR signaling response to resistance exercise is altered by chronic resistance training and detraining in skeletal muscle', *American Journal of Physiology-Heart and Circulatory Physiology*.

Ogasawara, R. *et al.* (2016) 'The role of mTOR signalling in the regulation of skeletal muscle mass in a rodent model of resistance exercise', *Scientific reports*, 6, p. 31142.

Ono, Y. and Sakamoto, K. (2017) 'Lipopolysaccharide inhibits myogenic differentiation of C2C12 myoblasts through the Toll-like receptor 4-nuclear factor-κB signaling pathway and myoblast-derived tumor necrosis factor-α', *PloS one*, 12(7), p. e0182040.

Pagano, R. R. (2012) *Understanding statistics in the behavioral sciences*. Cengage Learning.

Passey, S. L. *et al.* (2016) 'Serum amyloid A induces Toll-like receptor 2-dependent inflammatory cytokine expression and atrophy in C2C12 skeletal muscle myotubes', *PloS one*, 11(1), p. e0146882.

Pedersen, B. K. *et al.* (2003) 'Searching for the exercise factor: is IL-6 a candidate?', *Journal of Muscle Research & Cell Motility*, 24(2–3), p. 113.

Pedersen, B. K. and Febbraio, M. A. (2012) 'Muscles, exercise and obesity: skeletal muscle as a secretory organ', *Nature Reviews Endocrinology*, 8(8), pp. 457–465.

Pigna, E. *et al.* (2016) 'Aerobic exercise and pharmacological treatments counteract cachexia by

modulating autophagy in colon cancer', *Scientific reports*, 6, p. 26991.

Pyrczak, F. (2016) *Making sense of statistics: A conceptual overview*. Routledge.

Ralston, E., Lu, Z. and Ploug, T. (1999) 'The organization of the Golgi complex and microtubules in skeletal muscle is fiber type-dependent', *Journal of Neuroscience*. Soc Neuroscience, 19(24), pp. 10694–10705.

Rauch, J. *et al.* (2011) 'The secret life of kinases: functions beyond catalysis', *Cell communication and signaling*. BioMed Central, 9(1), p. 23.

Richter, E. A., Kiens, B. and Wojtaszewski, J. F. P. (2008) 'Can exercise mimetics substitute for exercise?', *Cell metabolism*, 8(2), pp. 96–98.

Rose, A. J. *et al.* (2009) 'A Ca(2+)-calmodulin-eEF2K-eEF2 signalling cascade, but not AMPK, contributes to the suppression of skeletal muscle protein synthesis during contractions', *J Physiol*. Copenhagen Muscle Research Centre and Molecular Physiology Group, Department of Exercise and Sport Sciences, University of Copenhagen, Denmark. a.rose@dkfz.de, 587(Pt 7), pp. 1547–1563. doi: 10.1113/jphysiol.2008.167528.

Rudman, D. *et al.* (1990) 'Effects of human growth hormone in men over 60 years old', *New England Journal of Medicine*, 323(1), pp. 1–6.

Rudman, D. *et al.* (1991) 'Effects of human growth hormone on body composition in elderly men', *Hormone Research in Paediatrics*. Karger Publishers, 36(Suppl. 1), pp. 73–81.

Safdar, A., Saleem, A. and Tarnopolsky, M. A. (2016) 'The potential of endurance exercise-derived exosomes to treat metabolic diseases', *Nat Rev Endocrinol*. Department of Pediatrics, McMaster University, 1200 Main Street West, Hamilton, Ontario L8N 3Z5, Canada. Department of Medicine, McMaster University, 1280 Main Street West, Hamilton, Ontario L8S 4L8, Canada., 12(9), pp. 504–517. doi: 10.1038/nrendo.2016.76.

Showkat, M., Beigh, M. A. and Andrabi, K. I. (2014) 'mTOR signaling in protein translation regulation: implications in cancer genesis and therapeutic interventions', *Molecular biology international*. Hindawi, 2014.

Squire, J. M. (2016) 'Muscle contraction: Sliding filament history, sarcomere dynamics and the two Huxleys', *Global Cardiology Science and Practice*, 2016(2).

StataCorp (2017) 'Stata Statistical Software'. College Station, Texas: StataCorp LP.

Stevenson, E. J. *et al.* (2005) 'The transcriptional profile of a myotube starvation model of atrophy', *Journal of applied physiology*.

Sun, L. *et al.* (2013) 'The effects of endoplasmic reticulum stress response on duck decorin stimulate myotube hypertrophy in myoblasts', *Molecular and cellular biochemistry*. Springer, 377(1–2), pp. 151–161.

Taaffe, D. R. *et al.* (1994) 'Effect of recombinant human growth hormone on the muscle strength response to resistance exercise in elderly men', *The Journal of Clinical Endocrinology & Metabolism*. Oxford University Press, 79(5), pp. 1361–1366.

Terruzzi, I., Pellegatta, F. and Luzi, L. (2005) 'Differential p70S6k and 4E-BP1 regulation by insulin and amino acids in vascular endothelial and smooth muscle cells', *Acta diabetologica*. Springer, 42(3), pp. 139–146.

Trendelenburg, A. U. *et al.* (2009) 'Myostatin reduces Akt/TORC1/p70S6K signaling, inhibiting myoblast differentiation and myotube size', *American Journal of Physiology-Cell Physiology*.

Vander, A. J., Sherman, J. H. and Luciano, D. S. (2001) *Human physiology. The mechanisms of body*

function. eight.

Velloso, C. P. (2008) 'Regulation of muscle mass by growth hormone and IGF-I', *British journal of pharmacology*. Wiley Online Library, 154(3), pp. 557–568.

Waterlow, J. C., Garlick, P. J. and MILL, W. (1978) *Protein turnover in mammalian tissues and in the whole body*. Elsevier/North-Holland Biomedical Press, 335 Jan van Galenstraat, PO Box 211, 1000 AE Amsterdam, The Netherlands.

Welc, S. S. *et al.* (2012) 'Hyperthermia increases interleukin-6 in mouse skeletal muscle', *American Journal of Physiology-Cell Physiology*, 303(4), pp. C455–C466.

Wolin, K. Y. *et al.* (2009) 'Physical activity and colon cancer prevention: a meta-analysis', *British journal of cancer*, 100(4), pp. 611–616. Available at: https://www.ncbi.nlm.nih.gov/pmc/articles/PMC2653744/pdf/6604917a.pdf.

Wullschleger, S., Loewith, R. and Hall, M. N. (2006) 'TOR signaling in growth and metabolism', *Cell*. Elsevier, 124(3), pp. 471–484.

Yaffe, D. and Saxel, O. R. A. (1977) 'Serial passaging and differentiation of myogenic cells isolated from dystrophic mouse muscle', *Nature*, 270(5639), pp. 725–727.

Appendices

Appendix 1: preparation of reagents

PBS

1 PBS tablet (Fisher, Fair Lawn, New Jersey, USA) in 100mL ddH_2O

Exo1

Exo1 purchased from Sigma Aldrich, UK

Molecular weight: 273.26

5mg stock

Solubility in DMSO: 19mg/mL

5mg in 1.83mL DMSO=10mM stock

Used a final concentration of 20µM

IGF-1

IGF-1 purchased from Sigma Aldrich, UK

Stock preparation: 1mg powder diluted in 100µL HCl (10mM)

Stock concentration: 1mg/mL

A 1:100 dilution in sterile PBS is prepared for a final concentration of 10 000ng/mL (4µL IGF-1 + 396µL PBS)

A working concentration of 10ng/mL will be used in the experiments.

Homogenisation buffer

For 100mL homogenisation buffer, pH 7.5

Tris-HCl (MP Biomedicals, Solon, Ohio) 0.788g

EDTA (Sigma, UK) 0.0372g

EGTA (Sigma, UK) 0.0380g

B-Glycerophosphate (Sigma, UK) 0.216g

NaF (Sigma, UK) 0.2g

Add 25µL sodium orthovanadate, 200Mm (Sigma, UK) + 1 tablet protease inhibitor tablet EDTA free (Roche, Manheim, Germany) in 10 mL homogenisation buffer

Laemmli SDS sample buffer

For 10mL Laemmli sample buffer

1M Tris-HCl (MP Biomedicals, Solon, Ohio) pH 6.8 2.4mL

20% sodium dodecyl sulphate (Fisher, Fair Lawn, New Jersey, USA) 3mL

Glycerol (Courtin & Warner LTD, Lewes, East Sussex, England) 3mL

Bromophenol Blue (Fisher, Fair Lawn, New Jersey, USA) 0.006g

On the day of usage, add 1.6mL 2-Mercaptoethanol (Sigma, UK) in 10mL Laemmli buffer

Transfer buffer

For 1L Transfer buffer

Tris base (Fisher, Fair Lawn, New Jersey, USA) 3.03g

Glycine (Fisher, Fair Lawn, New Jersey, USA) 14.4g

Methanol (Fisher, Fair Lawn, New Jersey, USA) 200mL

Top up to 1L with ddH_2O

TBST

For 1L 10x TBST, pH 7.6:

NaCl (Sigma, UK) 80g

Tris base (Fisher, Fair Lawn, New Jersey, USA) 24.2g

Tween-20 (Sigma, UK) 10mL

Top up to 1L with ddH_2O

Working concentration: 1x

Coomassie stain

For 50mL Coomassie stain

Methanol (Fisher, Fair Lawn, New Jersey, USA) 20mL

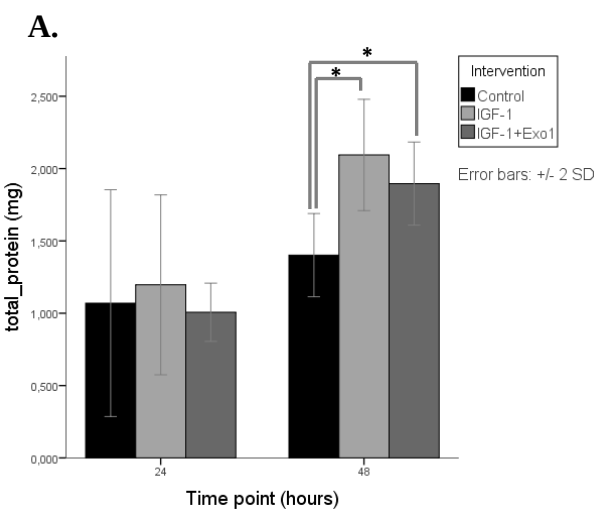
Acetic acid (VWR Chemicals, Fontanay-sous bois France) 5mL

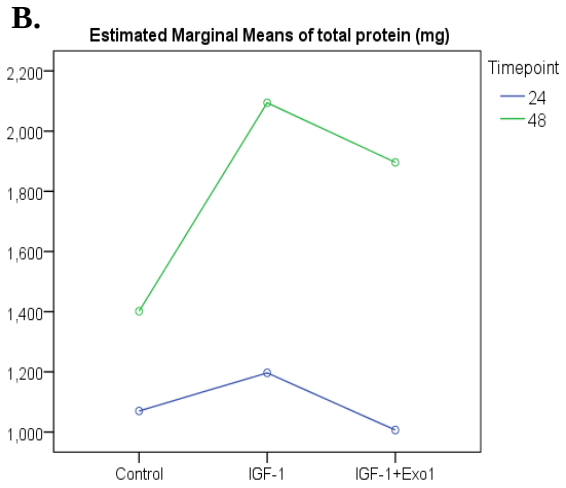
Brilliant blue (Sigma, UK) 0.05g

Top up to 50mL with H_2O

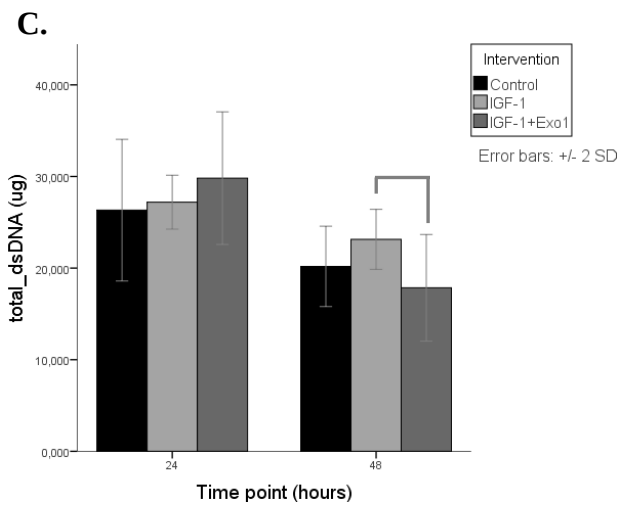
Appendix 2: protein/DNA analysis

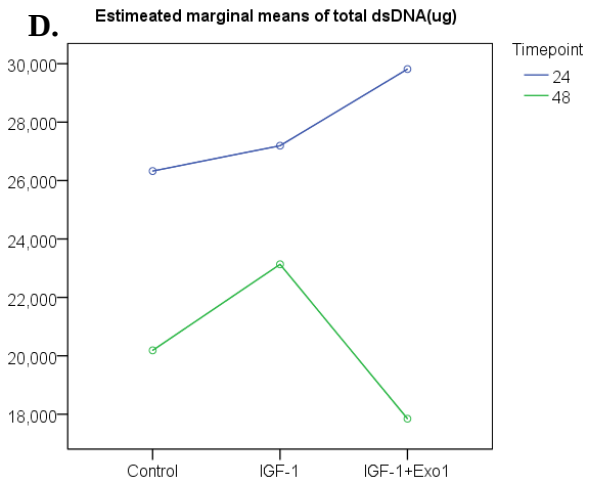
Total protein



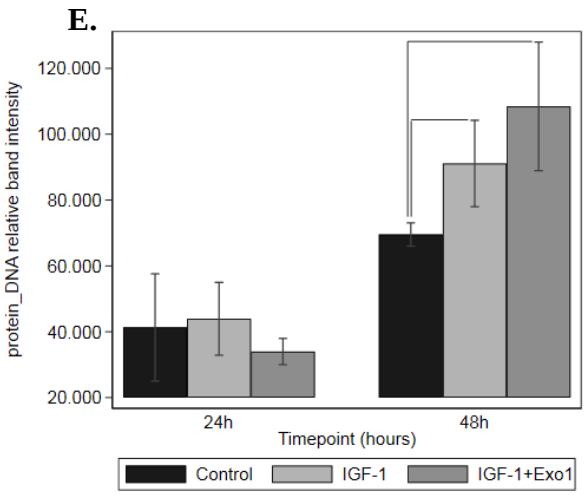


Total dsDNA





protein/DNA



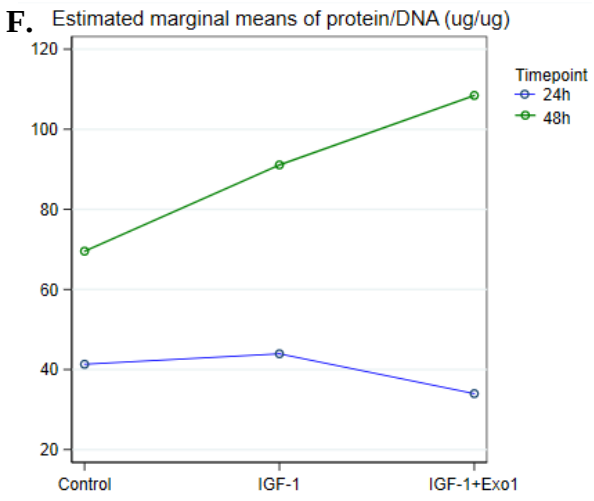


Figure 5 Total protein, total DNA and protein/DNA ratio analysis following IGF-1±Exo1 treatment. [A]Total protein expression (mg). [B] Estimated marginal means for total protein expression (mg). [C] Total double stranded DNA expression (µg). [D] Estimated marginal means for total dsDNA expression (µg). [E] protein/DNA ratio (µg/µg). [F] Estimated marginal means for protein/DNA ratio (µg/µg).

Appendix 3: Estimated marginal means of western blotting and myotube width results.

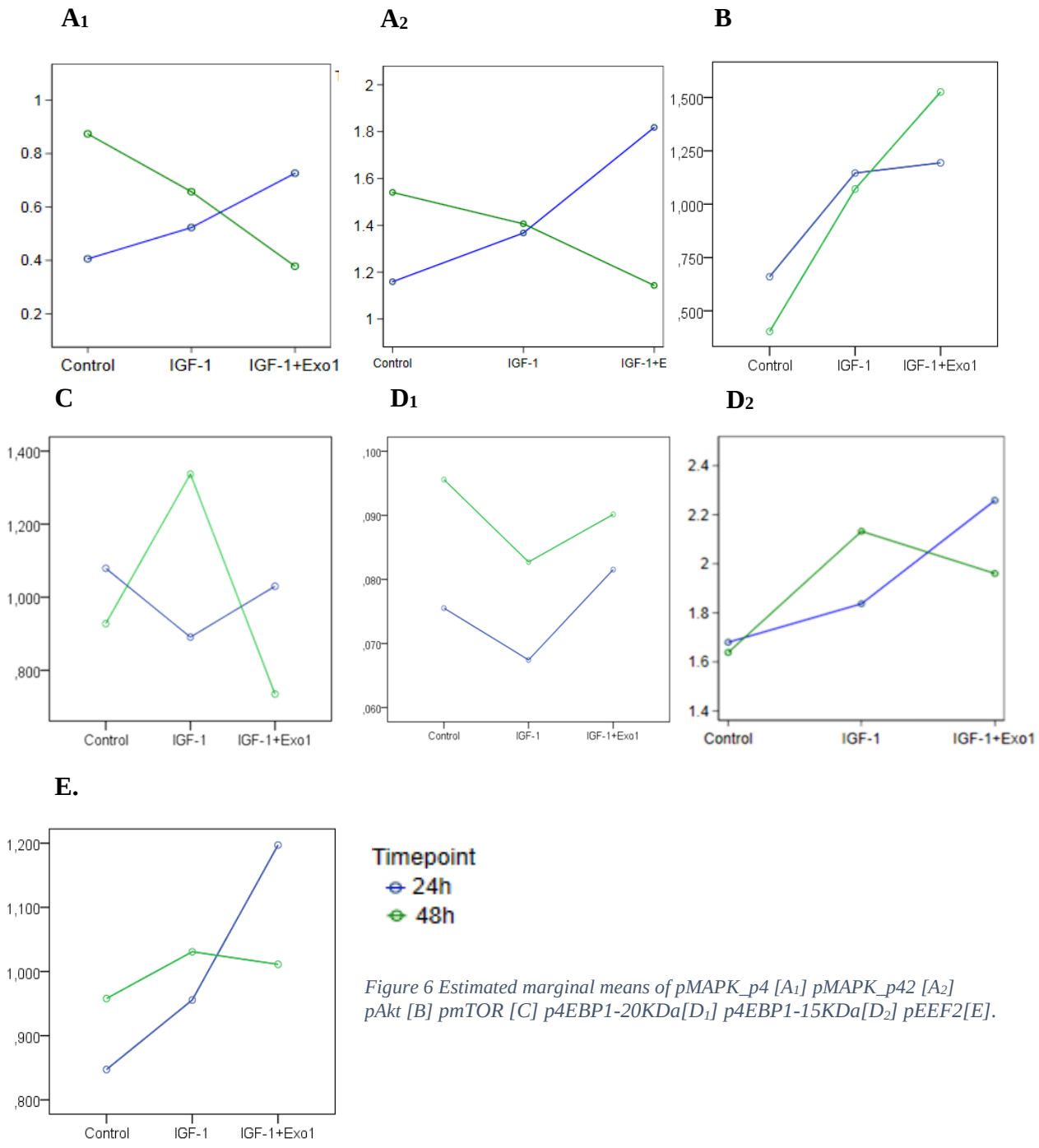


Figure 6 Estimated marginal means of pMAPK_p4 [A_1] pMAPK_p42 [A_2] pAkt [B] pmTOR [C] p4EBP1-20KDa[D_1] p4EBP1-15KDa[D_2] pEEF2[E].

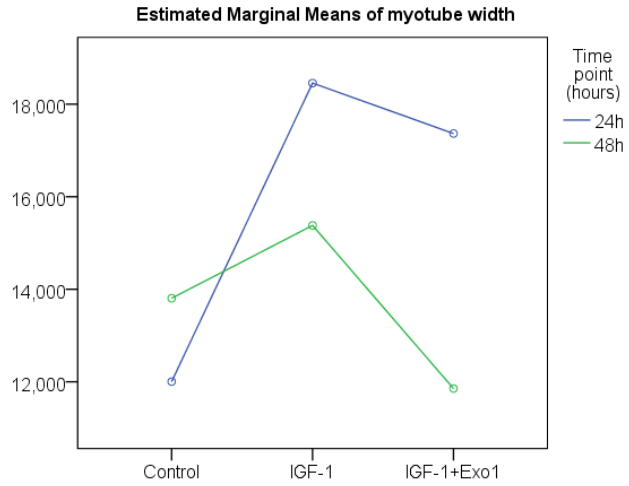


Figure 7 Estimated marginal means of myotube width following IGF-1±Exo1 treatment.

